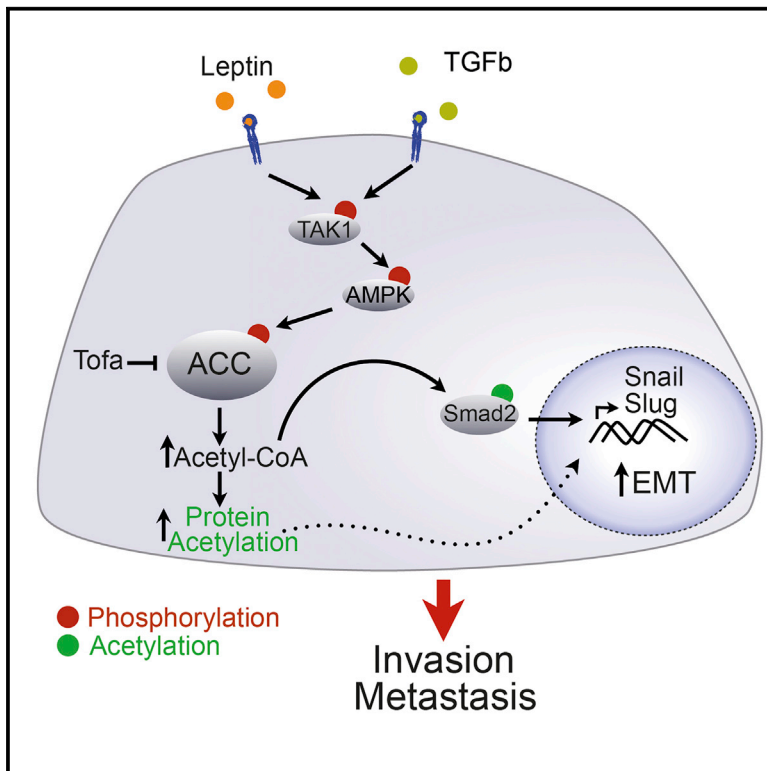


Cell Metabolism

Acetyl-CoA Carboxylase 1-Dependent Protein Acetylation Controls Breast Cancer Metastasis and Recurrence

Graphical Abstract



Authors

Marcos Rios Garcia,
Brigitte Steinbauer,
Kshitij Srivastava, ..., Peter P. Nawroth,
Stephan Herzig, Mauricio Berriel Diaz

Correspondence

stephan.herzig@helmholtz-muenchen.de
(S.H.),
mauricio.berrieldiaz@
helmholtz-muenchen.de (M.B.D.)

In Brief

Rios Garcia et al. identify the lipogenic enzyme ACC1 as a point of convergence for EMT and invasion-promoting pathways in mouse and human breast tumors. ACC1 inactivation by leptin or TGFβ signaling, both increased in obesity, drives invasion and metastasis of breast cancer cells through elevated acetyl-CoA and protein acetylation.

Highlights

- Leptin and TGFβ inhibit ACC1 through TAK1-AMPK signaling in breast cancer
- Inhibition of ACC1 elevates acetyl-CoA, and induces Smad2 acetylation and EMT
- Blocking the leptin-ACC1 axis counteracts metastasis formation in breast cancer
- Inactive pACC1 levels were increased in human breast cancer metastases

Acetyl-CoA Carboxylase 1-Dependent Protein Acetylation Controls Breast Cancer Metastasis and Recurrence

Marcos Rios Garcia,^{1,2,3,4} Brigitte Steinbauer,⁵ Kshitij Srivastava,⁶ Mahak Singhal,⁶ Frits Mattijssen,^{1,2,3,4} Adriano Maida,^{1,2,3,4} Sven Christian,⁷ Holger Hess-Stumpp,⁷ Hellmut G. Augustin,⁶ Karin Müller-Decker,⁵ Peter P. Nawroth,^{1,2,3,4} Stephan Herzig,^{1,2,3,4,8,*} and Mauricio Berriel Diaz^{1,2,3,4,*}

¹Institute for Diabetes and Cancer, Helmholtz Center Munich, Neuherberg, Germany

²Joint Heidelberg-IDC Translational Diabetes Program, Inner Medicine 1, Heidelberg University Hospital, Heidelberg, Germany

³Technical University Munich, 85764 Neuherberg, Germany

⁴Deutsches Zentrum für Diabetesforschung, 85764 Neuherberg, Germany

⁵Core Facility Tumor Models

⁶Division of Vascular Oncology and Metastasis

German Cancer Research Center (DKFZ) and Medical Faculty Mannheim, Heidelberg University, 69120 Heidelberg, Germany

⁷Division Tumor Metabolism and Hypoxia, Bayer Health Care, 13353 Berlin, Germany

⁸Lead Contact

*Correspondence: stephan.herzig@helmholtz-muenchen.de (S.H.), mauricio.berrieldiaz@helmholtz-muenchen.de (M.B.D.)

<https://doi.org/10.1016/j.cmet.2017.09.018>

SUMMARY

Breast tumor recurrence and metastasis represent the main causes of cancer-related death in women, and treatments are still lacking. Here, we define the lipogenic enzyme acetyl-CoA carboxylase (ACC) 1 as a key player in breast cancer metastasis. ACC1 phosphorylation was increased in invading cells both in murine and human breast cancer, serving as a point of convergence for leptin and transforming growth factor (TGF) β signaling. ACC1 phosphorylation was mediated by TGF β -activated kinase (TAK) 1, and ACC1 inhibition was indispensable for the elevation of cellular acetyl-CoA, the subsequent increase in Smad2 transcription factor acetylation and activation, and ultimately epithelial-mesenchymal transition and metastasis induction. ACC1 deficiency worsened tumor recurrence upon primary tumor resection in mice, and ACC1 phosphorylation levels correlated with metastatic potential in breast and lung cancer patients. Given the demonstrated effectiveness of anti-leptin receptor antibody treatment in halting ACC1-dependent tumor invasiveness, our work defines a “metabolocentric” approach in metastatic breast cancer therapy.

INTRODUCTION

Metabolic reprogramming during tumorigenesis is a well-accepted process indispensable for supporting the energy demands associated with rapid tumor cell proliferation. Different aspects of cell metabolism can be affected by this metabolic reprogramming, most notably aerobic glycolysis. The energy generated through aerobic glycolysis is thought to be sufficient to cover the energy

demands associated with cancer cell division and allow accumulation of biosynthetic precursors needed for anabolic reactions (Vander Heiden et al., 2009). In contrast to the dependence of cancer cells on aerobic glucose utilization, *de novo* fatty acid (FA) synthesis was proposed as a mechanism by which tumor cells become independent of extracellular lipids. Since FA synthase (FASN) was identified as the tumor antigen OA-519 in aggressive breast cancer (Currie et al., 2013; Kuhajda et al., 1994), numerous studies have confirmed the importance of FA biosynthesis for cancer cell growth and survival (Currie et al., 2013; Röhrig and Schulze, 2016; Santos and Schulze, 2012). Despite the fact that FASN seems to be of great importance in metastasis as well as primary tumors, this issue has recently been questioned in several publications (Jiang et al., 2015; Ríos et al., 2013), indicating that *de novo* FA synthesis reprogramming in cancer is far from being fully elucidated.

In the *de novo* FA synthesis pathway, the carbons of glucose after being converted to acetyl-CoA are used to synthesize malonyl-CoA by acetyl-CoA carboxylase (ACC) 1. ACC1 represents a key enzyme, as it is highly regulated by phosphorylation and allosteric regulation, providing a rapid adaptation to new micro-environmental conditions (Brownsey et al., 2006). This regulation is important as malonyl-CoA is not only necessary for *de novo* FA synthesis, but also determines the activity of carnitine palmitoyltransferases (CPTs), which couple acyl chains to carnitine for transport into the mitochondrial matrix and subsequent degradation by β -oxidation.

Previous studies have linked ACC1 and protein acetylation in yeast and mouse liver to metabolic adaptations (Chow et al., 2014; Galdieri and Vancura, 2012). However, little is known about the role of ACC1 beyond its functions in FA metabolism in non-tumor cells.

Breast cancer is the second leading cause of cancer mortality among women in the United States (<https://www.cdc.gov/cancer/dcpc/data/women.htm>). Around 15% of patients with breast cancer develop metastatic disease, and distant metastases are responsible for 90% of breast cancer-associated deaths

(Weigelt et al., 2005). Of note, breast cancer aggressiveness and high recurrence rates, in particular, have been linked to obesity in large epidemiological cohorts, and obesity-related metabolic dysfunction has emerged as a main risk factor to developing metastatic breast cancer in post-menopausal women (Khandekar et al., 2011). In the face of the pandemic dimension of obesity, the metabolic etiology of particularly metastatic breast cancer is expected to significantly rise over the next decades (Protani et al., 2010; Yung and Ligibel, 2016). However, treatment options have made little improvements and remain limited (Chaffer and Weinberg, 2011; Tevaarwerk et al., 2013). In this respect, the present studies report for the first time a role of ACC1 in suppressing breast cancer migration and invasion by an FA synthesis-independent, but acetyl-CoA-dependent, impact on the epithelial-mesenchymal transition (EMT) programs in breast tumor cells and its subsequent importance for tumor invasion and recurrence.

RESULTS

Leptin Induces Metastatic Behavior by Inhibition of ACC1

As obesity is typically characterized by aberrant levels of adipokines, including leptin (Rajala and Scherer, 2003), we initially aimed to explore the impact of obesity-related metabolic cues on breast tumor cell behavior. To this end, we analyzed the effect of leptin on proliferation, migration, or invasion in murine 4T1 and e0771 or human MDA-MB-231, MCF-7, and T47D breast cancer cell lines. As shown in Figures S1A–S1C, we were unable to detect changes in proliferation under leptin treatment in different breast cancer cell lines, despite readily detectable expression of both leptin and the leptin receptor (LepR) mRNA. However, a consistent effect on EMT and invasion was observed under leptin treatment conditions (Figures S1D–S1O). To test whether leptin indeed was involved in breast cancer metastasis *in vivo*, we performed a tumor resection experiment using wild-type or LepR knockdown 4T1 cells in mouse transplantation experiments. 4T1 cells were orthotopically implanted into the mammary fat pads of wild-type mice, and primary tumors were resected once they had reached a 5 mm diameter. Three weeks after tumor removal, lungs were collected and macro- and micro-metastases were counted. In line with our *in vitro* results, LepR knockdown cells showed a reduced metastatic capacity *in vivo* (Figures 1A and 1B). Moreover, an LepR blocking antibody inhibited invasion induced by leptin *in vitro* (Figure 1C) and reversed EMT upon antibody treatment of tumor-carrying animals *in vivo* (Figures 1D and S1P), indicating that LepR antibodies could be of interest as a co-adjuvant therapy in the treatment of patients with breast cancer after primary tumor resection.

To test if these cellular processes were coupled to metabolic alterations, we performed seahorse analyses upon leptin treatment in MDA-MB-231, MCF-7, 4T1, and e0771 tumor cells carrying either control or anti-LepR short hairpin RNA (shRNA) lentiviruses. Interestingly, leptin treatment increased the oxidative capacity of human and murine breast cancer cell lines, and this effect could be abolished by LepR knockdown (Figures 1E and 1F).

To monitor potential downstream metabolic targets of leptin signaling in these cells, we assessed total and pACC1^{Ser79} levels

as leptin has been shown to exert different effects on ACC1 depending on the tissue context, either by reducing ACC1 phosphorylation (Gao et al., 2007) or by inducing an inhibitory ACC1 phosphorylation at serine 79 (Minokoshi et al., 2002). As shown in Figures 1G and S1I, all cell lines investigated increased the levels of ACC1 phosphorylation under leptin treatment, and this effect was inhibited in LepR knockdown cells. Increased levels of malonyl-CoA resulting from impaired ACC1 action inhibit the activity of CPT-1, which is involved in FA oxidation (Foster, 2012). In line with this observation, leptin increased CPT-1 activity, leading to an increase in FA oxidation (Figure 1H). We hypothesized that CPT-1 might be one of the factors underlying the effects of leptin on tumor cell behavior; however, CPT-1 inhibition with etomoxir in e0771 cells did not show any effects on invasion (Figure 1I), indicating that FA oxidation is not necessary for leptin-dependent invasive behavior.

In order to test if ACC1 inhibition could be involved in leptin effects in breast cancer cells, we decided to inhibit ACC1 in LepR knockdown cells. Remarkably, pharmacological ACC1 inhibition with the specific inhibitor Tofa in e0771 cell line was not only able to rescue the effect of LepR knockdown on invasion, but also triggered invasiveness in LepR wild-type cells (Figure 1J).

Collectively, these data favored the hypothesis that ACC1 phosphorylation and inhibition are a necessary step in leptin-promoted EMT in breast cancer, and that the mechanism is independent of FA oxidation.

ACC1 Inhibition Increases Acetyl-CoA Levels, Total Protein Acetylation, and Metastases in Breast Cancer Cells

As EMT was regulated by ACC1 activity and ACC1 is generally involved in malonyl-CoA synthesis, thereby consuming acetyl-CoA as a substrate, we hypothesized that inhibition of ACC1 during EMT upon leptin treatment can affect levels of acetyl-CoA and protein acetylation in breast cancer cells. To test this concept, we analyzed the levels of total protein acetylation in a number of breast tumor cells treated with leptin. As shown in Figures 2A, S2A, and S2B, cells treated with leptin displayed increased total protein acetylation, the effect of which was commonly observed across all the cell lines tested. In agreement with a crucial role of ACC1 in mediating these effects, direct ACC1 inhibition by Tofa also increased total protein acetylation, and inhibition of p300 acetyltransferase activity blunted this effect (Figure 2B). Interestingly, in conjunction with protein acetylation, Tofa and leptin also increased the levels of EMT markers, and p300 inhibition reduced this effect (Figures 2C and S2C). While both leptin and Tofa treatment increased acetyl-CoA levels in cells, LepR knockdown reduced acetyl-CoA levels only in leptin-stimulated, but not in Tofa-treated, cells (Figure 2D), in line with a function of ACC1 activity downstream of LepR signaling. These data indicated that ACC1 inhibition is directly involved in changes in total protein acetylation and induction of EMT.

To further validate the role of ACC1 activity in the regulation of protein acetylation and EMT induction, we investigated the effect of ACC1 knockdown in 4T1 breast cancer cells. ACC1 knockdown was sufficient to induce protein acetylation (as demonstrated by histone H3 acetylation) and to increase EMT markers, and this effect was independent of leptin treatment (Figure 2E). To confirm that ACC1 inhibition was, at least in part, under the

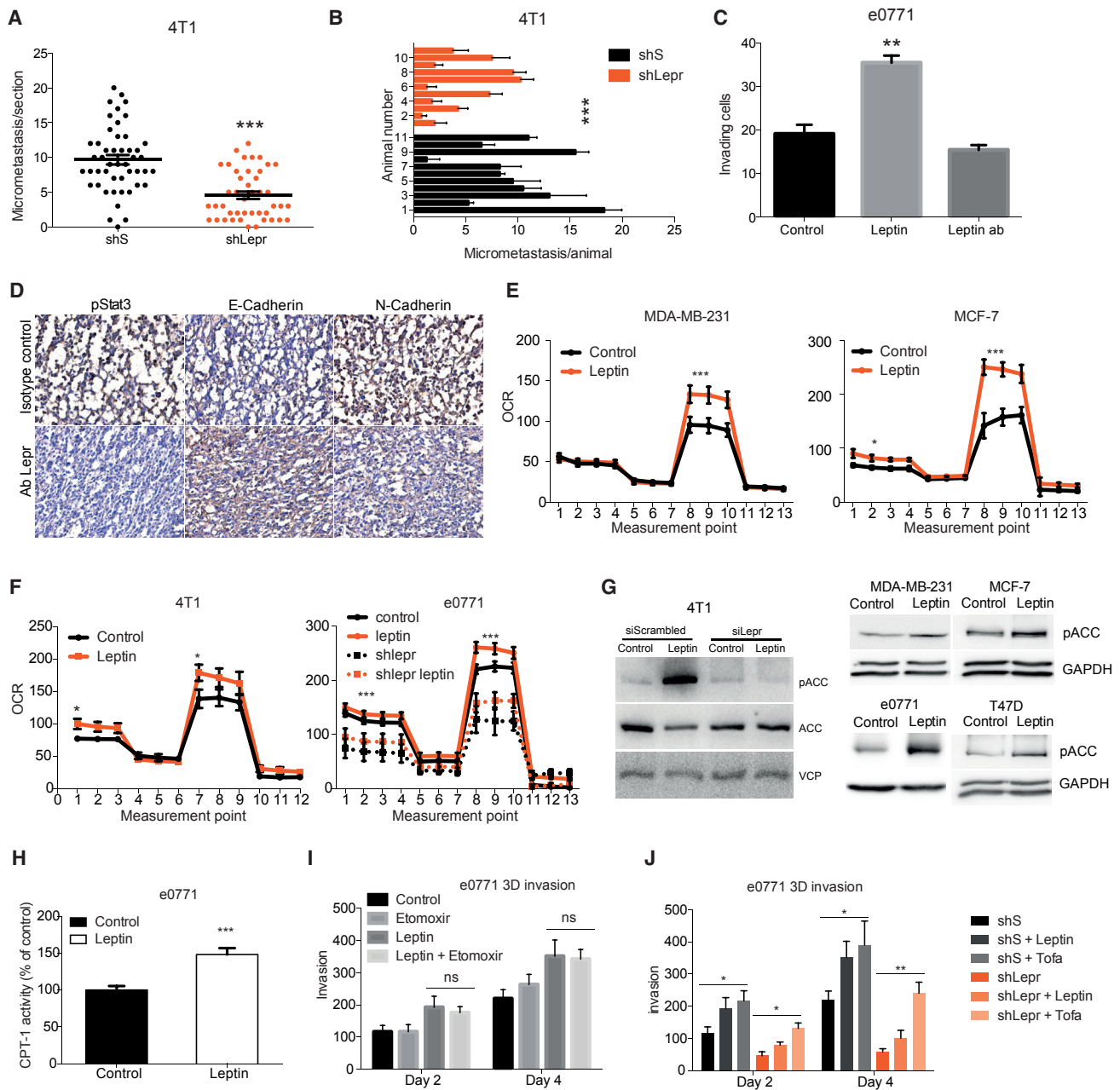


Figure 1. Leptin Increases ACC1 Phosphorylation and Oxidative Metabolism in Human and Murine Cancer Cell Lines

(A and B) *In vivo* lung micrometastasis of 4T1 cells carrying control or LepR shRNAs injected into BalbC mice, 3 weeks after primary tumor resection (n = 11). (C) Invasion of e0771 cells, treated with 100 ng/mL leptin alone or in combination with LepR antibody, in transwell assays (n = 3). (D) Representative IHC of primary tumors generated by orthotopical injection of e0771 in C57Bl6/J mice. Animals were treated twice a week with IgG control or LepR blocking antibody (10 mg/kg) until the end of the experiment. (E and F) Seahorse analysis of glucose oxidation in wild-type or LepR knockdown human (E) and murine breast cancer cell lines in the presence or absence of 100 ng/mL leptin (F) (n = 3). (G) Levels of ACC1 phosphorylation at serine 79, total ACC1, and VCP in tumor cells as indicated and treated with 100 ng/mL leptin (n = 6). (H) Relative levels of CPT-1 activity in e0771 cells treated with 100 ng/mL leptin (n = 3). (I) Three-dimensional invasion of e0771 cells treated with 100 ng/mL leptin, 10 μ M etomoxir, or the combination of both (n = 3). (J) Three-dimensional invasion of e0771 wild-type or LepR knockdown cells treated with 5 μ M Tofa (n = 3). All data in the figure are shown as the mean \pm SEM. n numbers refer to biological replicates. One-way ANOVA with Tukey's multiple comparison post-test (C, E, F, and I), Student's t test (A, B, and H), and two-way ANOVA with Bonferroni's multiple comparison post-test (J). *p < 0.05, **p < 0.01, ***p < 0.001. See also Figure S1.

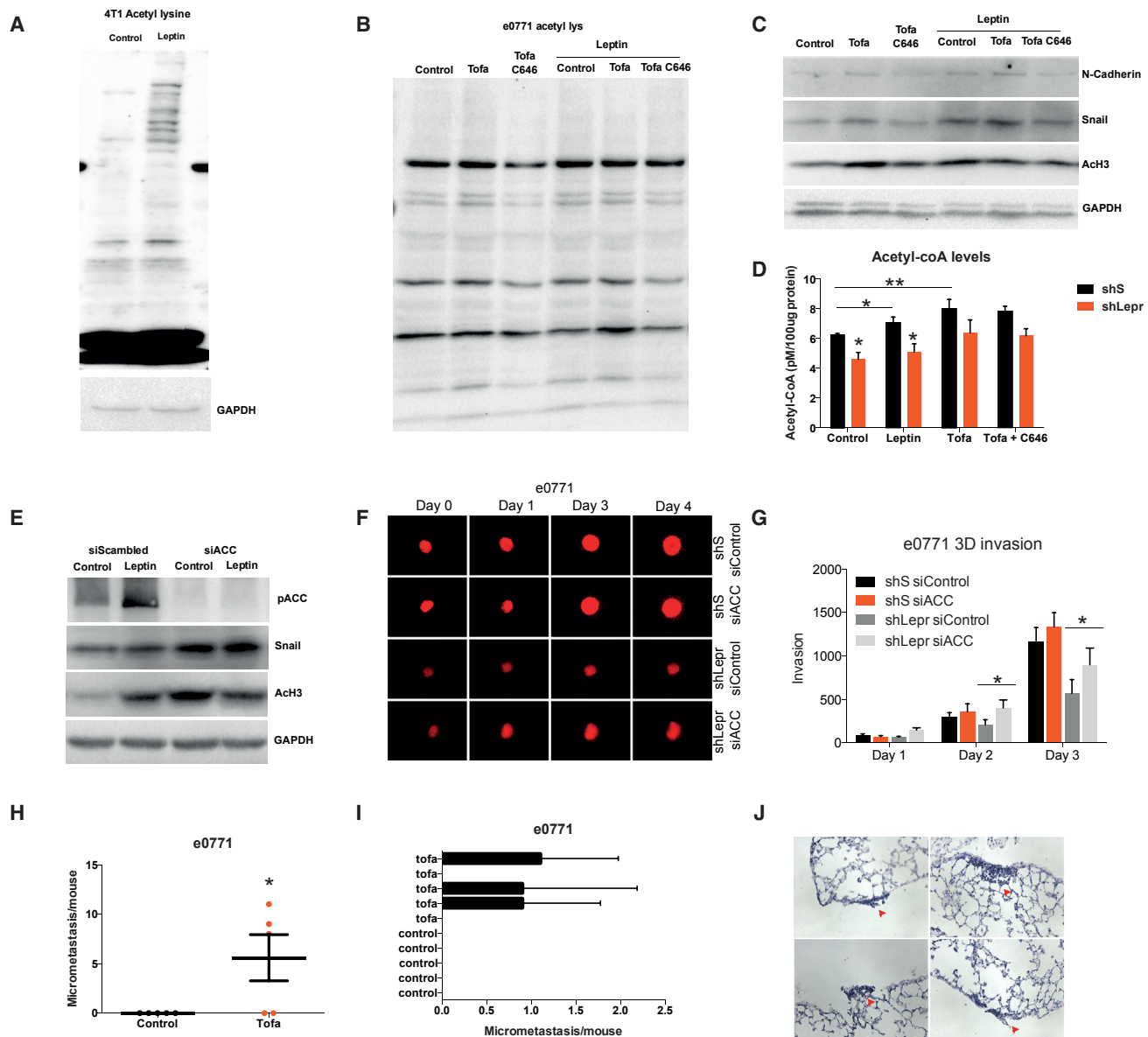


Figure 2. Leptin Inhibits ACC1 to Increase Total Protein Acetylation and Metastasis

(A) Levels of total protein acetylation in untreated or 100 ng/mL leptin-treated 4T1 cells (n = 3).
 (B) Total protein acetylation in e0771 wild-type or LepR knockdown cells treated with ACC1 inhibitor (5 μ M Tofa) or a p300 acetyltransferase inhibitor (C646) in the presence or absence of 100 ng/mL leptin (n = 3).
 (C) Protein levels of N-cadherin, Snail, and histone H3 acetylation in e0771 cells treated with 5 μ M Tofa or C646 in the presence or absence of 100 ng/mL leptin (n = 3).
 (D) Total acetyl-CoA levels in e0771 cells treated as in (B).
 (E) Protein levels of Snail and histone H3 acetylation in wild-type or ACC1 knockdown 4T1 cells treated with leptin (n = 4).
 (F and G) Representative pictures (F) and quantification (G) of migration of wild-type or LepR knockdown e0771 cells in combination with ACC1 knockdown (n = 4).
 (H–J) Number of micrometastases (H), number of micrometastases per animal (I), and representative pictures of the micrometastases (J) in lungs of C57Bl6/J mice injected with e0771 cells into the tail vein. Cells were treated for 48 hr with 5 μ M Tofa before injection (n = 5).
 All data in the figure are shown as the mean \pm SEM. n numbers refer to biological replicates. One-way ANOVA with Tukey's multiple comparison post-test (D and G) and Student's t test (H and I). *p < 0.05, **p < 0.01, ***p < 0.001. See also Figure S2.

control of leptin during EMT, we performed 3D invasion assays. Knockdown of ACC1 was able to rescue the reduced invasion in LepR-deficient 4T1 and e0771 cells (Figures 2F, 2G, and S2D). Consistent with these observations, a 48 hr pre-incubation of

the non-metastatic breast cancer cell line e0771 with Tofa to inhibit ACC1 was sufficient to induce lung colonization after tail vein injection of these pre-treated cells into wild-type mice (Figures 2H–2J), altogether demonstrating that ACC1 inhibition

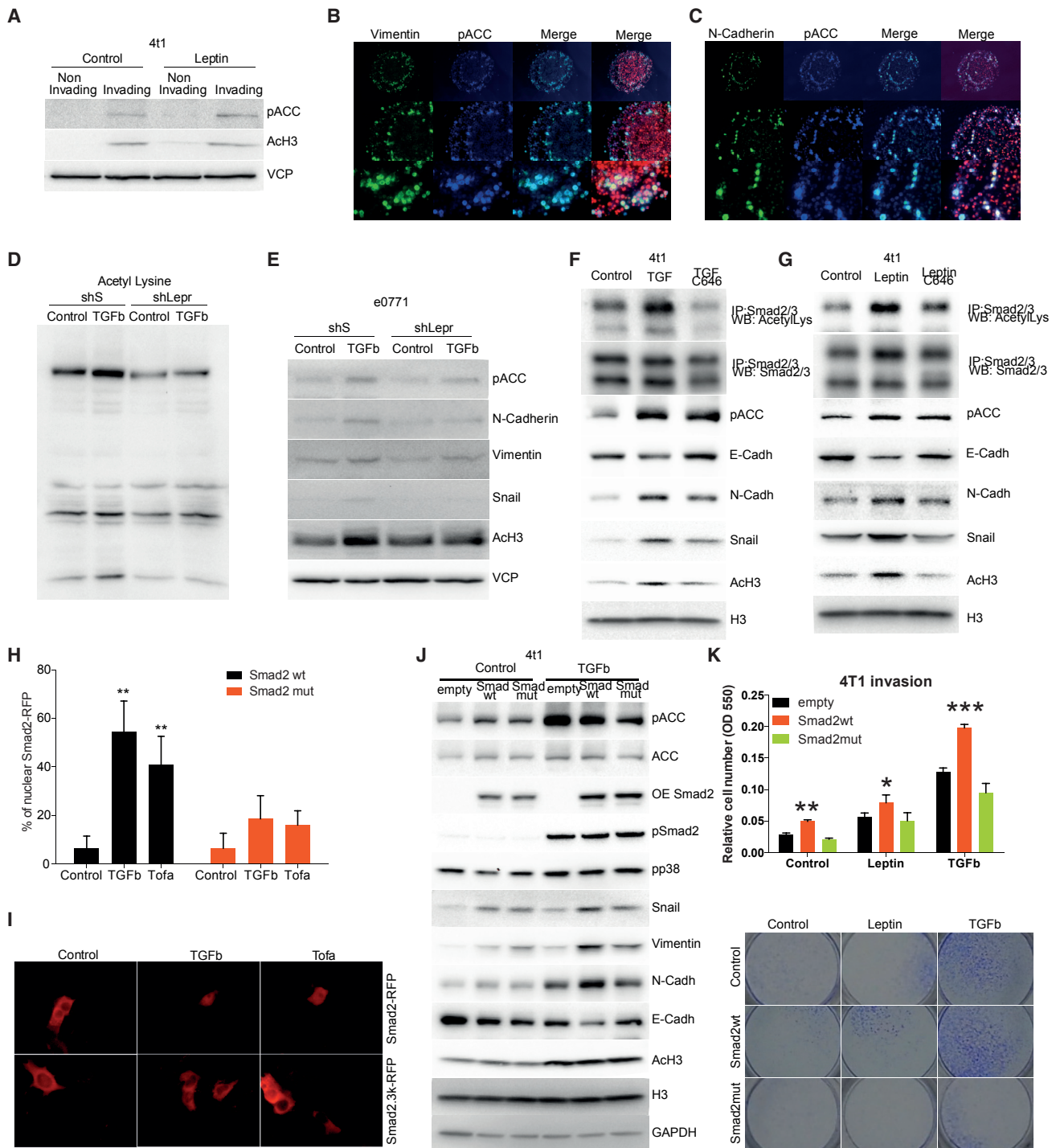


Figure 3. Leptin and TGFβ Inhibit ACC1, Increasing Smad2 Acetylation Levels

(A) Levels of pACC1 and histone H3 acetylation in 4T1 separated invading and non-invading cells obtained from transwell inserts (n = 3).
 (B and C) Immunofluorescence of e0771 3D spheroids showing (B) vimentin (green), pACC1 (blue), and nucleus (red), or (C) N-cadherin (green), pACC1 (blue), and nucleus (red) (n = 2).
 (D and E) Levels of total protein acetylation (D) and EMT markers, pACC1, and histone H3 acetylation (E) in control or LepR shRNA-carrying e0771 cells treated with TGFβ for 24 hr (n = 3).
 (F and G) Immunoprecipitation of 4T1 cells treated with TGFβ and C646 (F) or leptin and C646 (G) showing levels of Smad2 acetylation (n = 3). The same samples were analyzed by western blot to check levels of histone H3 acetylation and EMT markers.
 (H and I) Quantification (H) and representative microphotograph (I) showing Smad2 localization in 4T1 cells transfected with RFP-Smad2 wild-type or RFP-Smad2K3R and treated 4 hr with TGFβ or Tofa (n = 3).

(legend continued on next page)

regulated invasion *in vitro* and *in vivo*, and that this effect was related to an increase in general cellular protein acetylation.

Phosphorylation-Dependent ACC1 Inhibition Is a Common Point of Convergence for EMT-Inducing Signals in Breast Tumors

To test whether the upregulation of ACC1 phosphorylation is a more global mechanism during EMT beyond leptin signaling, we evaluated the levels of pACC1 in invading and non-invading 4T1 cells obtained from transwell inserts. ACC1 phosphorylation, as well as histone H3 acetylation, was more prominently detectable in invading cells as compared with non-invading ones, both in the presence and absence of leptin (Figure 3A). We also determined ACC1 phosphorylation in 3D invasion assays by immunofluorescence in e0771 spheroids. As shown in Figures 3B and 3C, pACC1 was mainly present in cells localized in the invading area of the spheroids. More interestingly, expression of the key EMT markers vimentin and N-cadherin perfectly matched cells with high ACC1 phosphorylation status, suggesting that ACC1 phosphorylation is a common event in invading cells.

To further validate this finding, we investigated the effect of TGF β (a well-known EMT inducer) on protein acetylation and ACC1 phosphorylation. To this end, we examined the TGF β effect in wild-type or LepR-deficient e0771 cells. Treatment with TGF β for 24 hr increased total protein acetylation in both wild-type and LepR knockdown cells and this increase correlated with the upregulation of pACC1 and EMT markers (Figures 3D, 3E, and S3A).

The TGF β canonical pathway involves regulation of Smad transcription factors, and Smad2/3 phosphorylation and nuclear translocation were previously found to cause EMT (Lamouille et al., 2014). Also, both Smads can be acetylated and this acetylation controls their transcriptional activity (Simonsson et al., 2006; Tu and Luo, 2007). Thus, we hypothesized that ACC1 inhibition and the elevation of cellular acetyl-CoA levels followed by EMT in breast cancer cells occur in a Smad acetylation-dependent manner. To test this idea, we performed immunoprecipitation experiments in 4T1 cells treated with leptin, TGF β , and Tofa in combination with the p300 acetyltransferase inhibitor C646. TGF β treatment increased Smad2 acetylation as previously shown (Figure 3F). Interestingly, leptin and Tofa treatment also increases Smad2 acetylation (Figures 3G and S3B), and under these treatments (TGF β , leptin, and Tofa), the p300 inhibitor was able to reduce these levels, together with a decrease in EMT markers, without affecting Smad2 phosphorylation (Figures 3F, 3G, and S3B). These data indicated that Smad2 acetylation was responsible, at least in part, for the EMT induction by ACC1 inhibition.

To further validate the role of Smad2 acetylation in the context of EMT induction by ACC1 phosphorylation, we generated a mutant Smad2 that cannot be acetylated. As previously described (Tu and Luo, 2007), overexpression of the acetyla-

tion-deficient RFP-Smad2 fusion protein in HEK293T cells was sufficient to reduce EMT markers in TGF β -treated cells (Figure S3C). Similarly, Smad2mut expression counteracted the induction of EMT marker levels upon Tofa treatment (Figure S3C). To confirm the importance of Smad2 acetylation in breast cancer during the EMT process, we overexpressed the different Smad2 constructs in 4T1 breast cancer cells. After TGF β or Tofa treatment for 4 hr, we observed that RFP-Smad2 localized in the nucleus of the cells; however, TGF β and Tofa were unable to induce this nuclear translocation in cells expressing mutant RFP-Smad2K3R (Figures 3H and 3I). Western blot analysis of 4T1 cells overexpressing the acetylation-deficient RFP-Smad2 fusion protein showed a reduction in Vimentin, Snail, and N-cadherin together with increased levels of E-cadherin under conditions of leptin or TGF β stimulation in comparison with Smad2 wild-type cells (Figures 3J and S3D). Finally, to confirm the effect of Smad2 mutant on EMT, we performed transwell invasion assays under these conditions, showing that 4T1 cells expressing acetylation-deficient RFP-Smad2 were less invasive than those expressing wild-type Smad2 (Figure 3K). These data supported the notion that Smad2 acetylation is regulated by ACC1 activity in order to support/induce EMT in breast cancer cell lines under both leptin and TGF β treatment conditions.

As both TGF β and leptin regulate ACC1 phosphorylation, we next focused on the common signaling pathways downstream of TGF β and leptin to elucidate the signals involved in ACC1 phosphorylation during EMT induction. AMP-dependent kinase (AMPK) is a well-characterized upstream ACC1 kinase, and it was shown that it can be regulated by MEK/ERK, PI3K/AKT, and TGF β -activated kinase (TAK)1 (Mihaylova and Shaw, 2011). Interestingly, inhibitors for MEK and PI3K had minor effects on ACC1 phosphorylation or EMT marker expression, such as Snail, upon TGF β treatment in e0771 and 4T1 cells (Figures 4A and 4B). In contrast, a TAK1 inhibitor was found to completely blunt ACC1 phosphorylation and EMT marker induction in response to TGF β exposure, indicating that TAK1 was the main upstream pathway involved in ACC1 regulation and subsequent EMT in breast cancer cells (Figures 4A, 4B, and S4A). In agreement with this conclusion, overexpression of a constitutively active TAK1 mutant increased the levels of pACC1 and EMT markers as compared with control cells, reaching levels comparable to TGF β stimulation (Figure S4B). AMPK, the key kinase in ACC1 phosphorylation, can be activated by TAK1; however, LKB1 and CAMKK2B are the most studied kinases responsible for AMPK activation. To investigate which of these kinases is involved in the activation of the AMPK-ACC pathway during EMT, we performed knockdown experiments. Interestingly, knockdown of both LKB1 and CAMKK2B only had minor effects on basal levels of pACC1, as well as the increase of pACC1 and EMT markers induced by leptin and TGF β (Figures 4C, S4C, and S4D). In contrast, knockdown of TAK1 reduced the levels of pACC1 in MCF-7 cells, the effect of which was associated with a decrease in EMT markers in cells treated

(J) Smad2 phosphorylation and EMT markers in 4T1 cells transfected with empty vector, RFP-Smad2 wild-type, or RFP-Smad2K3R and treated with Tofa.

(K and L) Transwell invasion assay showing the effect of empty vector, RFP-Smad2 wild-type, or RFP-Smad2K3R in 4T1 cells treated with leptin or TGF β (K) and representative microphotograph of the transwell membranes (L) (n = 2).

All data in the figure are shown as the mean \pm SEM. n numbers refer to biological replicates. One-way ANOVA with Tukey's multiple comparison post-test (H and K). *p < 0.05, **p < 0.01, ***p < 0.001. See also Figure S3.

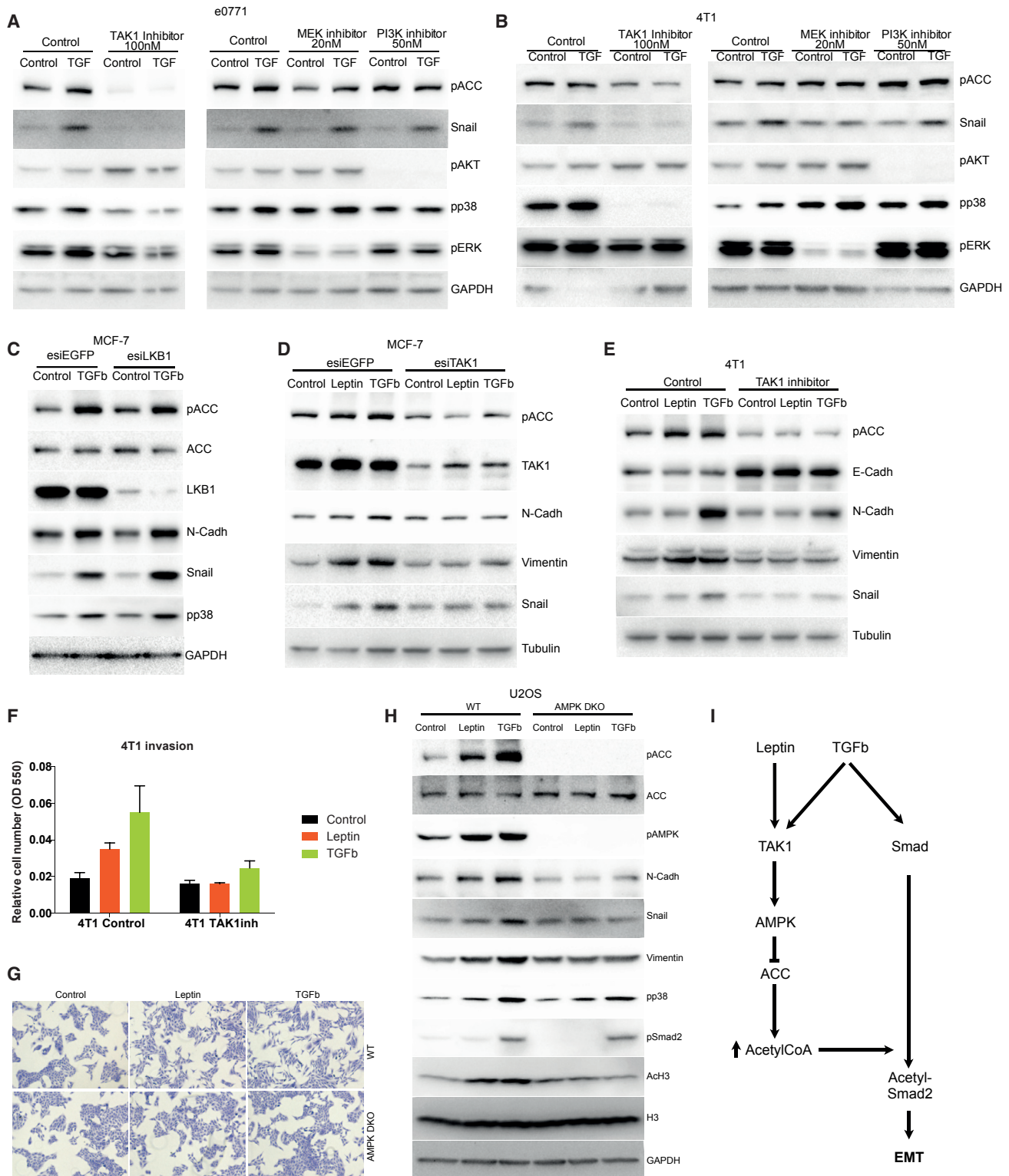


Figure 4. Leptin and TGFβ Phosphorylate ACC1 through TAK1-AMPK Pathway

(A and B) Western blots showing pACC1 and Snail in e0771 (A) or 4T1 cells treated with TGFβ in combination with TAK1, MEK1/2, and PI3K inhibitors (B) (n = 3). (C) Effect of LKB1 knockdown on ACC1 phosphorylation and EMT marker levels in MCF-7 cells treated with TGFβ (n = 3). Representative blots shown. (D) Western blot of MCF-7 cells transfected with esiEGFP or esiCAMKK2B and treated with leptin or TGFβ. (E) Western blot of 4T1 cells treated with leptin or TGFβ in combination with TAK1 inhibitor (100 nM) showing levels of different EMT markers and pACC. (F) Quantification of transwell invasion assay of 4T1 cells treated as in (E) (n = 2).

(legend continued on next page)

with leptin or TGF β (Figure 4D). Moreover, TAK1 inhibitor treatment prevented the increase in pACC1, EMT markers, and invasion in 4T1 cells treated with leptin or TGF β (Figures 4E and 4F). To elucidate if AMPK was the kinase involved in ACC1 phosphorylation during EMT in breast cancer cell lines, we performed experiments knocking down AMPK α subunits. Knockdown of AMPK α 1 was sufficient to abrogate the induction of EMT markers by both leptin and TGF β treatment (Figure S4E). The knockdown of AMPK α 2 had only minor effects, indicating that AMPK α 1 was the major isoform expressed in our cells. In order to include an additional model to confirm the role of AMPK in ACC1 phosphorylation during EMT, we used an osteosarcoma cell line (U2OS) harboring a previously described double knockout (DKO) of the two catalytic subunits AMPK α 1 and AMPK α 2 (Toyama et al., 2016), as the AMPK wild-type version of these cells has been shown to respond to leptin treatment by increasing ACC1 phosphorylation (Malik et al., 2011). After leptin or TGF β treatment, U2OS wild-type cells showed increased levels of pACC1, histone H3 acetylation, and EMT markers as we previously observed in breast cancer cell lines (Figure 4H). AMPK α DKO U2OS cells had lower basal levels of EMT markers and histone H3 acetylation compared to AMPK wild-type cells. In fact, AMPK α DKO U2OS cells showed only a marginal increase in EMT markers under leptin or TGF β treatment, indicating that AMPK is required for EMT induction in this context. Moreover, the lower levels of EMT markers in AMPK DKO U2OS cells were also reflected at the level of cell morphology (Figure 4G).

These data supported the idea that the ACC1-dependent control of cellular acetyl-CoA levels represents a key event in EMT and that ACC1 activity is inhibited in breast, and probably also other tumor cells, by leptin and TGF β signaling in a TAK1- and AMPK-dependent manner (Figure 4I).

ACC1 Activity Drives Breast Cancer Metastasis and Tumor Recurrence *In Vivo*

Since pharmacological ACC1 inhibition with Tofa increased tumor cell lung colonization *in vivo* (Figures 2H–2J), we next aimed to confirm our findings by genetic approaches. To directly test the effect of ACC1 activity on metastasis, we first generated a panel of ACC1 knockdown cells, including 4T1, e0771, MDA-MB-231, MCF-7, and T47, by shRNA-carrying lentivirus infection. All cell lines showed an increase in EMT markers and histone H3 acetylation in correlation with low levels of ACC1 (Figures 5A and S5A). Moreover, transwell invasion assays showed that ACC1 knockdown was sufficient to increase invasion (Figure 5B). We further investigated the effect of ACC1 knockdown in an *in vivo* metastasis model by injecting low metastatic murine and human cell lines into the tail vein of wild-type mice. Intriguingly, both ACC1-depleted e0771 and MCF-7 cells showed an increase in lung colonization as compared with ACC1 wild-type cells (Figures 5C, 5D, and S5B), confirming that the reduction of ACC1 activity was able to increase invasion *in vitro* and metastasis *in vivo*.

As ACC1 knockdown increased EMT in breast cancer cell lines, we next investigated if the increase in EMT was a consequence of the acetyl-CoA accumulation or due to other effects upon reduction of *de novo* FA synthesis. ATP-citrate lyase (ACLY) generates acetyl-CoA from citrate, which is then further used by ACC1 for malonyl-coA synthesis. In line with the important role of acetyl-coA levels for EMT regulation, the knockdown of ACLY in MCF-7 cells was sufficient to reduce EMT markers as well as invasion. Also, loss of ACLY rescued the EMT marker levels induced by the knockdown of ACC1 and completely blunted the invasive activity of the cells (Figures 5E and 5F). Moreover, U2OS wild-type and AMPK α DKO cells treated with Tofa increased EMT markers and invasion, and ACLY inhibition reduced these effects (Figures 5G–5I). Taken together, these data demonstrated that acetyl-CoA levels in tumor cells are regulated by metastatic signals through ACC1 to support EMT, and also suggested that ACLY inhibition might represent an alternative therapeutic intervention point to reduce metastasis.

Pharmacological and genetic inhibition of ACC1 increased the metastatic capacity of breast cancer cells, thus prompting us to analyze the invasion and metastatic capabilities of cells with increased ACC1 activity. To this end, we generated 4T1 and MDA-MB-231 cells with stable expression of wild-type ACC1 (ACC^{S79}), constitutively active ACC1 (ACC^{S79A}), or constitutively inactive (phospho-mimic) ACC^{S79E}, validated by measurements of ACC1 activity (Figure S5C). The two cell lines generated displayed identical growth properties as compared with wild-type cells (Figure S5D; data not shown). However, morphological changes were evident (Figure S5E), and cells overexpressing ACC1 showed reduced EMT marker expression, indicated by reduced Snail and induced E-cadherin levels, most notably in ACC^{S79A}-expressing cells (Figures 5J and S5H). While cells expressing ACC^{S79} had the ability to phosphorylate and inhibit ACC1 activity, ACC^{S79A}-expressing cells did not and consequently treatment with leptin or TGF β did not increase EMT markers or invasion in these ACC^{S79A}-carrying cells (Figures 5J, 5K, and S5H). Of note, overexpression of the constitutively inactive ACC^{S79E} had no effect on EMT marker levels and invasion (Figures S5F and S5G). Notably, the capacity of the cells expressing different ACC1 constructs to increase EMT markers or invasion was associated with the acetyl-CoA concentrations in the respective cells (Figure 5L).

As hypoxia can also induce EMT in breast cancer cells, we studied the effect of hypoxia in ACC^{S79A}-carrying cells. Consistent with other EMT-inducing cues, ACC^{S79A}-expressing cells were unable to increase EMT markers when compared with control cells during hypoxia (Figure S5I), suggesting that ACC1 inhibition might be a common mechanism necessary to support metastasis formation.

Furthermore, we studied the effect of ACC1 overexpression in metastasis *in vivo* by injecting the highly metastatic cell line 4T1 orthotopically in congenic mice using cells expressing either

(G) Representative microphotograph showing morphological changes of U2OS wild-type or AMPK DKO treated with leptin and TGF β .

(H) Effect of leptin and TGF β on EMT markers in U2OS wild-type or AMPK DKO cells (n = 4).

(I) Proposed mechanism of EMT regulation by leptin and TGF β .

All data in the figure are shown as the mean \pm SEM. n numbers refer to biological replicates. One-way ANOVA with Tukey's multiple comparison post-test (F). *p < 0.05, **p < 0.01, ***p < 0.001. See also Figures S4 and S5.

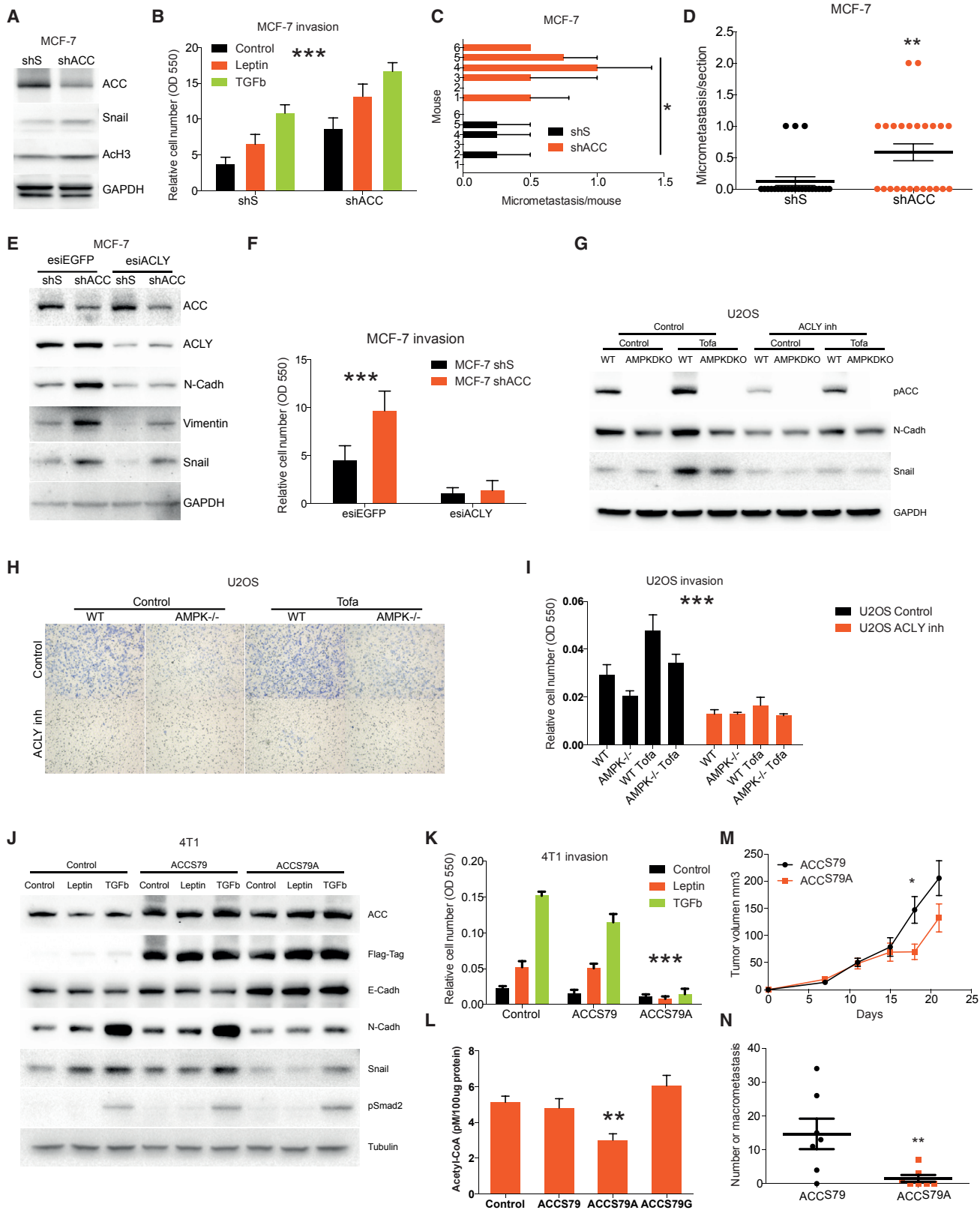


Figure 5. ACC1 Regulates Metastatic Capacity of Breast Cancer Cells Lines In Vitro and In Vivo

(A) Western blot of MCF-7 cells carrying control or ACC1 shRNA showing Snail and histone H3 acetylation levels (n = 2).
 (B) Transwell assay of MCF-7 shScrambled or shACC1 cells treated with leptin or TGFβ (n = 2).

(legend continued on next page)

ACC^{S79} or ACC^{S79A}. Interestingly, 3 weeks after primary tumor resection, animals injected with ACC^{S79A}-expressing cells showed a significantly smaller number of lung metastases as compared with ACC^{S79}-expressing cells (Figure 5N). Also, ACC^{S79A}-expressing cells showed a small reduction in tumor growth that was not observed *in vitro* (Figure 5M). Of note, the number of metastases in the ACC^{S79} group increased in relation to primary tumor size, while in the ACC^{S79A} group the number of metastases was independent from primary tumor size, confirming that ACC^{S79A} cells had reduced metastatic capacity *in vivo* (Figure S5J). These data demonstrated the critical role of ACC1 in metastasis formation, and supported the idea that ACC1 inhibition is a necessary step as well as a driver signal in the metastatic process.

ACC1 Phosphorylation Is Induced in Metastasis of Human Breast Cancer

To finally validate our results in human settings, we compared normal tissue, primary tumor, and metastasis samples from the same patient in human tissue microarrays (TMAs). A significant increase in pACC1 was detected in primary breast tumors as compared with corresponding normal tissue as well as in metastases compared to primary tumors (Figures 6A and 6B). Additional analysis of the data revealed a progressive increase in ACC1 phosphorylation from normal breast tissue to metastasis independent of the tumor grade. Representative images for pACC1 immunohistochemistry (IHC) from breast cancer TMAs and the used score index are shown in Figure 6D. Consistent with our previous observations, ACC1 phosphorylation was markedly increased in metastases as compared with normal tissue and primary tumors (Figure 6C). Moreover, N-cadherin and pp38, an established marker of EMT (del Barco Barrantes and Nebreda, 2012), were increased in metastases compared with primary tumors and in primary tumors compared with normal tissue; however, E-cadherin showed an inverse regulation (Figures 6E–6G). Remarkably, we found positive correlation between the levels of pACC1 and N-cadherin, and even more prominently between pACC1 and pp38 (Figures 6H and 6I), suggesting that our *in vitro* findings are reflecting the situation in human breast tumors and metastases.

Finally, in order to see if the dysregulation of ACC1 may be common to other tumors, we studied the levels of pACC1 in human lung tissue, primary tumor, and corresponding metastases. Interestingly, ACC1 phosphorylation was significantly increased from normal lung tissue to primary tumors and from

primary tumor to metastases (Figures 6J and 6K). Moreover, as in human breast cancer, lung tumors showed a progressive increase in pACC1 independent of the tumor grade (Figure 6L).

Collectively, these data indicated that inhibition of ACC1 by phosphorylation is a critical feature of metastasis and aggressive behavior not only in human breast cancer, but also in lung adenocarcinoma, and could probably be extended to other tumor entities.

DISCUSSION

Metastatic tumor recurrence imposes a major threat upon patients with breast cancer (Early Breast Cancer Trialists' Collaborative Group (EBCTCG), 2005; Khandekar et al., 2011) and is currently further increasingly promoted by obesity-related metabolic dysfunction at the population level (Protani et al., 2010; Yung and Ligibel, 2016). Aberrant adipokine and cytokine signaling represents one of the key features of obese metabolism. Indeed, both leptin and TGF β levels are significantly elevated in obese patients and proportionally increase with the degree of adiposity (Rajala and Scherer, 2003), and elevated leptin signaling has been linked to breast cancer aggressiveness and prognosis in epidemiological studies (Guo et al., 2012; Wu et al., 2009).

Our current study now defines the inhibition of the key lipogenic enzyme ACC1 as a molecular point of convergence for EMT and invasion-promoting pathways, including both leptin and TGF β , in breast cancer cells. Most notably, both leptin and TGF β were found to suppress ACC1 function in breast tumor cells by inhibitory phosphorylation partly mediated by the TAK1 kinase. We propose here that by reducing ACC1 activity, tumor cells display an increase in total acetyl-CoA levels, protein acetylation, migration, and invasion, triggered through an enhanced activation of EMT-inducing Smad2 transcription factor acetylation. However, we cannot exclude other players in this regulation due to the changes observed in total protein acetylation as a consequence of ACC1 phosphorylation, and further investigation should be done to address this question. As ACC1 phosphorylation is also increased in human metastatic tissue as compared with primary tumors or normal breast and lung tissue, our data suggest that the ACC1-dependent metabolic reprogramming represents a conserved feature in cancer metastases formation and tumor recurrence. Of note, the ACC1 dependence seems to hold true for all major breast cancer sub-types, as estrogen receptor-positive and also highly aggressive triple-negative tumor cells were similarly affected by ACC1 inhibition, further strengthening the

(C and D) Lung micrometastases quantification per animal (C) or in total (D), induced by MCF-7 cells carrying control or ACC1 shRNA injected into the tail veins of nude mice (six mice per group).

(E and F) Western blot of MCF-7 shScrambled or shACC1 cells transfected with esiEGFP or esiACLY showing changes in EMT markers (E) and transwell invasion assay (F) (n = 2).

(G) Effect of Tofa alone or in combination with an ACLY inhibitor on EMT markers in U2OS wild-type or AMPK DKO cells (n = 3).

(H and I) Representative microphotograph (H) and quantification (I) of transwell invasion assay of U2OS cells treated as in (G) (n = 2).

(J) Western blot of 4T1 cells transfected with empty vector, ACC1 wild-type, or ACC1^{S79A} in the presence or absence of leptin or TGF β showing levels of EMT markers (n = 3).

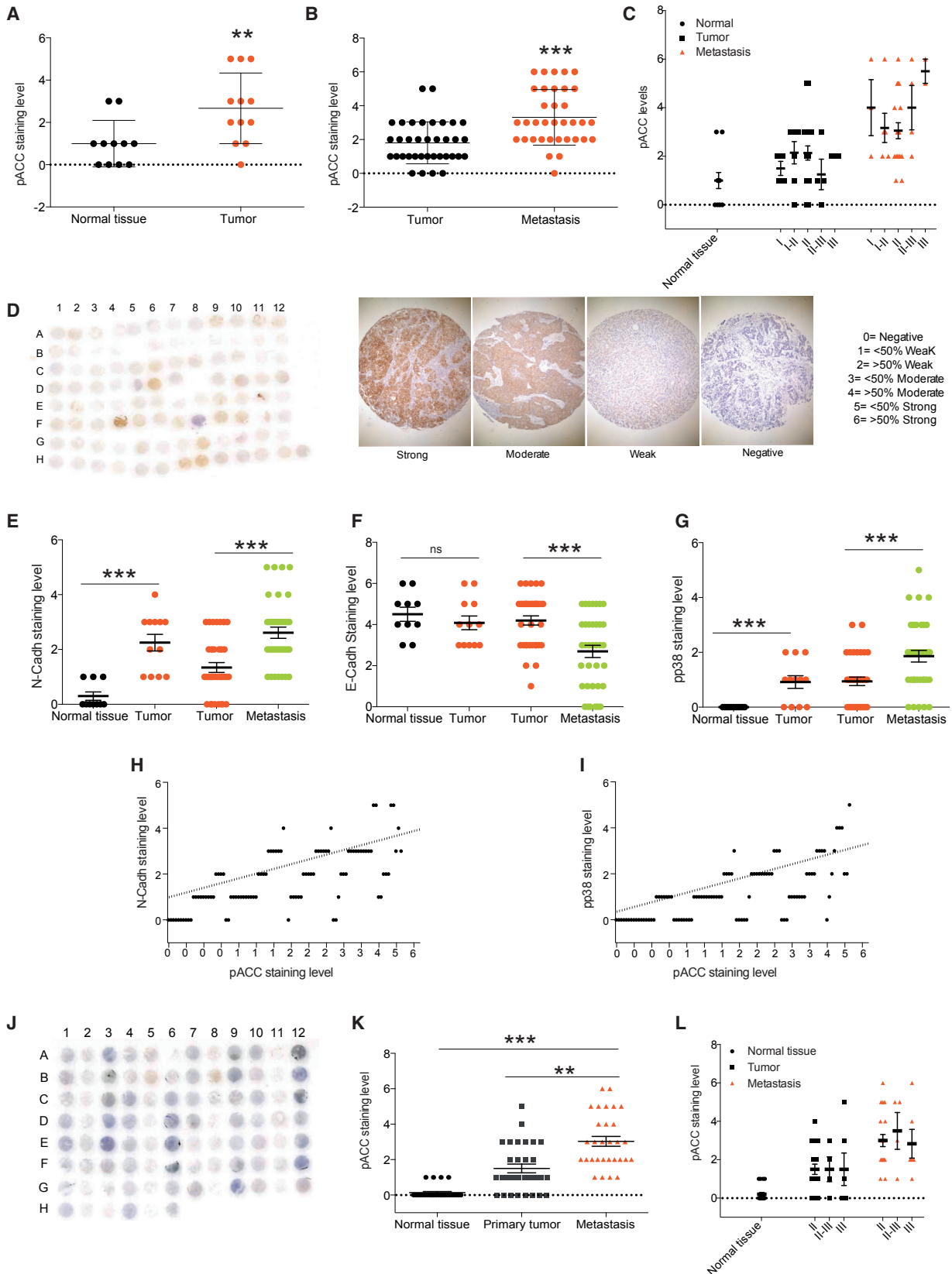
(K) Transwell invasion assay quantification of 4T1 ACC1 wild-type or ACC1^{S79A} cells treated with leptin or TGF β (n = 2).

(L) Acetyl-CoA levels in 4T1 ACC1 wild-type, ACC1^{S79A}, or ACC1^{S79A} cells.

(M) Primary tumor growth curve of 4T1 cells carrying wild-type ACC1 or ACC1^{S79A} injected into the mammary fat pad of BalbC mice.

(N) Lung micrometastases induced by same cells as in (F), 3 weeks after primary tumor resection (seven mice per group).

All data in the figure are shown as the mean \pm SEM. n numbers refer to biological replicates. One-way ANOVA with Tukey's multiple comparison post-test (B, F, I, K, and M) and Student's t test (D and N). *p < 0.05, **p < 0.01, ***p < 0.001.



(legend on next page)

speculation that ACC1-dependent tumor cell aggressiveness represents a rather conserved biological feature.

Metabolic pathways have been relatively well studied in cancer initiation and progression, and *de novo* FA synthesis has been defined as a mechanism in cancer cells to become independent from extracellular lipids and support high proliferation rates (Currie et al., 2013; Röhrig and Schulze, 2016; Santos and Schulze, 2012). In the case of ACC, an FA oxidation-dependent function in cell proliferation and lung tumorigenesis was described previously that relied on the maintenance of cellular NADPH levels through ACC activity (Jeon et al., 2012). However, relatively little is still known about ACC function in tumor cells and the literature data are often contradictory (Luo et al., 2017; Svensson et al., 2016). Along these lines, FASN knockdown or inhibition was described to reduce tumor cell growth (Currie et al., 2013; Röhrig and Schulze, 2016; Santos and Schulze, 2012), but it was also shown that the FASN knockdown can induce metastasis by affecting *de novo* FA synthesis (Jiang et al., 2015). Intriguingly, in the present study the ACC1-triggered EMT and tumor recurrence in breast cancer seems not to be related to its activity in the FA synthesis pathway, but rather relies on its regulatory function for cellular acetyl-CoA levels and ultimately modifies transcription factors by post-translational modifications, thereby providing a previously not described enzymatic mechanism in EMT regulation. Thus, we speculate that knockdown of FASN increases EMT by a similar mechanism, in which acetyl-CoA accumulation and protein acetylation are the major players.

It has been previously shown that AMPK activation (which inhibits ACC1) interferes with EMT (Chou et al., 2014; Li et al., 2016), while we here report an increase in ACC1 phosphorylation in invading cells as well as in cells treated with the EMT inducers leptin and TGF β . Moreover, we show here that AMPK α 1 knockdown and AMPK α DKO cells displayed a reduction in EMT markers and invasion. This discordancy is likely explained by the fact that previous studies have mainly focused on the activation of AMPK by compounds such as AICAR and metformin, which in turn are known to decrease levels of acetyl-CoA in cells as ACC1 activation does (Griss et al., 2015; Wang et al., 2016; Wu et al., 2013). Thus, it will be interesting to study in the future whether the activation of specific AMPK complexes could reduce EMT and acetyl-CoA levels in tumor cells, which will shed further light on the relative importance of this mechanism in tumor cell invasive behavior.

Since its first identification in yeast (Galdieri and Vancura, 2012), increased levels of acetyl-CoA and total protein acetylation by ACC1 inhibition have been found only in liver-specific ACC1

knockout mice that show high acetylation levels of metabolic enzymes (Chow et al., 2014). In this respect, the deregulation of protein acetylation, specifically histone modification, has been observed in different cancer types, and acetate can be used as a precursor of acetyl-CoA to promote cancer cell survival in hypoxia stress conditions by increasing *de novo* FA synthesis through histone acetylation (Gao et al., 2016). However, none of these previous studies have gone into a specific mechanism in which a physiological or pathophysiological signal regulates acetyl-CoA through ACC1 phosphorylation in order to affect cellular behavior. Our findings now demonstrate that ACC1 inhibition during EMT increases acetyl-CoA levels and total protein acetylation in breast cancer cells, whereas constitutively active ACC1 reduces acetyl-CoA as it does to EMT markers. As ACLY knockdown or inhibition not only reduces EMT in wild-type cells, but also in cells treated with Tofa or knockdown for ACC1, we speculate that the regulation of acetyl-CoA by both enzymes is a key step highly regulated in cancer cells to support EMT. Overall, our data indicate that ACC1 activation may be an approach to suppress breast cancer metastasis. However, as it was previously shown that ACC1 inhibition reduces tumor cell proliferation (Brusselmans et al., 2005; Chajès et al., 2006; Svensson et al., 2016), any ACC1 modulation should be well balanced in terms of timing during a therapeutic regimen. In contrast, ACLY inhibition can be the more interesting approach from a therapeutic point of view, as previous works have shown that ACLY inhibition reduces tumor growth (Zaidi et al., 2012), and here we observe that it also can reduce EMT. Nevertheless, our tumor resection/recurrence studies indicate that ACC1 activation could specifically serve as a (neo)-adjuvant therapy following primary tumor resection, thereby halting tumor metastases formation and recurrence in these patients. It is tempting to speculate that an antibody-based therapy targeting TAK1 induction may well serve this purpose, given the principal effectiveness of both LepR inhibition and antibody delivery in reversing EMT markers and breast tumor cell invasive behavior. Our study now paves the way for the development of “metabolo-centric” approaches toward the prevention of tumor recurrence in breast cancer by targeting the ACC1-dependent EMT axis.

STAR METHODS

Detailed methods are provided in the online version of this paper and include the following:

- KEY RESOURCES TABLE
- CONTACT FOR REAGENT AND RESOURCE SHARING

Figure 6. ACC1 Phosphorylation Status Increases from Normal to Metastatic Breast Tissue in Humans

(A and B) IHC staining of pACC1 in normal human mammary gland and corresponding primary tumors (A) or primary tumor and corresponding metastases (B). (C) IHC staining of pACC1 in normal tissue, primary tumor, and corresponding metastasis in relation to tumor grade. pACC1 IHC staining of LepR in normal mammary gland and corresponding primary tumor, or primary tumor and corresponding metastases. (D) Representative image of the human breast cancer TMA IHC and score index used to quantify levels of pACC1. (E–G) IHC staining of N-cadherin (E), E-cadherin (F), or pp38 (G) in normal tissue, primary tumor, and corresponding metastasis in human breast cancer TMA. (H) Correlation of N-cadherin and pACC1 staining levels in human breast cancer TMA ($R^2 = 0.2881$). (I) Correlation of pp38 and pACC1 staining levels in human breast cancer TMA ($R^2 = 0.3543$). (J) Image of the human lung adenocarcinoma TMA IHC. (K) IHC stainings of pACC1 in normal human lung, corresponding primary tumors, and corresponding metastases. (L) IHC staining of pACC1 in normal tissue, primary tumor, and corresponding metastasis in relation to tumor grade. All data in the figure are shown as the mean \pm SEM. One-way ANOVA with Tukey’s multiple comparison post-test (C, E–G, K, and L) and Student’s t test (A and B). * $p < 0.05$, ** $p < 0.01$, *** $p < 0.001$.

● EXPERIMENTAL MODEL AND SUBJECT DETAILS

- Animal Studies
- Cell Culture
- TMA

● METHOD DETAILS

- Cell Treatments
- Animal Studies
- Transfection and Infection
- Migration/Invasion Assays
- Soft Agar Assays
- Western Blot and Immunoprecipitation
- Immunohistochemistry and Immunofluorescence
- CPT-1 and ACC1 activity
- Seahorse Analyses
- Acetyl-CoA Measurements

● QUANTIFICATION AND STATISTICAL ANALYSIS

- Statistical Analysis

SUPPLEMENTAL INFORMATION

Supplemental Information includes five figures and can be found with this article online at <https://doi.org/10.1016/j.cmet.2017.09.018>.

AUTHOR CONTRIBUTIONS

M.R.G., F.M., A.M., B.S., K.S., M.S., S.C., and H.H.-S. performed experiments and generated experimental tools. K.M.-D. and H.G.A. supervised the tumor resection experiments. P.P.N., M.B.D., and S.H. designed and directed research, and M.R.G., S.H., and M.B.D. wrote the manuscript.

ACKNOWLEDGMENTS

We thank T. Schafmeier for comments on the manuscript. This work was supported by grants from the DKFZ-Bayer Cooperation Program and the HGF Future Topic “Aging and Metabolic Re-programming” to S.H.

Received: February 10, 2017

Revised: July 18, 2017

Accepted: September 20, 2017

Published: October 19, 2017

REFERENCES

Boehm, J.S., Zhao, J.J., Yao, J., Kim, S.Y., Firestein, R., Dunn, I.F., Sjöström, S.K., Garraway, L.A., Weremowicz, S., Richardson, A.L., et al. (2007). Integrative genomic approaches identify IKBKE as a breast cancer oncogene. *Cell* **129**, 1065–1079.

Brownsey, R.W., Boone, A.N., Elliott, J.E., Kulpa, J.E., and Lee, W.M. (2006). Regulation of acetyl-CoA carboxylase. *Biochem. Soc. Trans.* **34**, 223–227.

Brusselmans, K., De Schrijver, E., Verhoeven, G., and Swinnen, J.V. (2005). RNA interference-mediated silencing of the acetyl-CoA-carboxylase- α gene induces growth inhibition and apoptosis of prostate cancer cells. *Cancer Res.* **65**, 6719–6725.

Chaffer, C.L., and Weinberg, R.A. (2011). A perspective on cancer cell metastasis. *Science* **331**, 1559–1564.

Chajès, V., Cambot, M., Moreau, K., Lenoir, G.M., and Joulin, V. (2006). Acetyl-CoA carboxylase α is essential to breast cancer cell survival. *Cancer Res.* **66**, 5287–5294.

Chou, C.C., Lee, K.H., Lai, I.L., Wang, D., Mo, X., Kulp, S.K., Shapiro, C.L., and Chen, C.S. (2014). AMPK reverses the mesenchymal phenotype of cancer cells by targeting the Akt-MDM2-Foxo3a signaling axis. *Cancer Res.* **74**, 4783–4795.

Chow, J.D., Lawrence, R.T., Healy, M.E., Dominy, J.E., Liao, J.A., Breen, D.S., Byrne, F.L., Kenwood, B.M., Lackner, C., Okutsu, S., et al. (2014). Genetic in-

hibition of hepatic acetyl-CoA carboxylase activity increases liver fat and alters global protein acetylation. *Mol. Metab.* **3**, 419–431.

Currie, E., Schulze, A., Zechner, R., Walther, T.C., and Farese, R.V., Jr. (2013). Cellular fatty acid metabolism and cancer. *Cell Metab.* **18**, 153–161.

del Barco Barrantes, I., and Nebreda, A.R. (2012). Roles of p38 MAPKs in invasion and metastasis. *Biochem. Soc. Trans.* **40**, 79–84.

Early Breast Cancer Trialists' Collaborative Group (EBCTCG) (2005). Effects of chemotherapy and hormonal therapy for early breast cancer on recurrence and 15-year survival: an overview of the randomised trials. *Lancet* **365**, 1687–1717.

Foster, D.W. (2012). Malonyl-CoA: the regulator of fatty acid synthesis and oxidation. *J. Clin. Invest.* **122**, 1958–1959.

Foty, R. (2011). A simple hanging drop cell culture protocol for generation of 3D spheroids. *J. Vis. Exp.* **2720**.

Galdieri, L., and Vancura, A. (2012). Acetyl-CoA carboxylase regulates global histone acetylation. *J. Biol. Chem.* **287**, 23865–23876.

Gao, S., Kinzig, K.P., Aja, S., Scott, K.A., Keung, W., Kelly, S., Strynadka, K., Chohann, S., Smith, W.W., Tamashiro, K.L., et al. (2007). Leptin activates hypothalamic acetyl-CoA carboxylase to inhibit food intake. *Proc. Natl. Acad. Sci. USA* **104**, 17358–17363.

Gao, X., Lin, S.H., Ren, F., Li, J.T., Chen, J.J., Yao, C.B., Yang, H.B., Jiang, S.X., Yan, G.Q., Wang, D., et al. (2016). Acetate functions as an epigenetic metabolite to promote lipid synthesis under hypoxia. *Nat. Commun.* **7**, 11960.

Griss, T., Vincent, E.E., Egnatchik, R., Chen, J., Ma, E.H., Faubert, B., Viollet, B., DeBerardinis, R.J., and Jones, R.G. (2015). Metformin antagonizes cancer cell proliferation by suppressing mitochondrial-dependent biosynthesis. *PLoS Biol.* **13**, e1002309.

Guo, S., Liu, M., Wang, G., Torroella-Kouri, M., and Gonzalez-Perez, R.R. (2012). Oncogenic role and therapeutic target of leptin signaling in breast cancer and cancer stem cells. *Biochim. Biophys. Acta* **1825**, 207–222.

Jeon, S.M., Chandel, N.S., and Hay, N. (2012). AMPK regulates NADPH homeostasis to promote tumour cell survival during energy stress. *Nature* **485**, 661–665.

Jiang, L., Xiao, L., Sugiura, H., Huang, X., Ali, A., Kuro-o, M., Deberardinis, R.J., and Boothman, D.A. (2015). Metabolic reprogramming during TGF β 1-induced epithelial-to-mesenchymal transition. *Oncogene* **34**, 3908–3916.

Kaczor, J.J., Ziolkowski, W., Popinigis, J., and Tarnopolsky, M.A. (2005). Anaerobic and aerobic enzyme activities in human skeletal muscle from children and adults. *Pediatr. Res.* **57**, 331–335.

Khandekar, M.J., Cohen, P., and Spiegelman, B.M. (2011). Molecular mechanisms of cancer development in obesity. *Nat. Rev. Cancer* **11**, 886–895.

Kuhajda, F.P., Jenner, K., Wood, F.D., Hennigar, R.A., Jacobs, L.B., Dick, J.D., and Pasternack, G.R. (1994). Fatty acid synthesis: a potential selective target for antineoplastic therapy. *Proc. Natl. Acad. Sci. USA* **91**, 6379–6383.

Lamouille, S., Xu, J., and Derynck, R. (2014). Molecular mechanisms of epithelial-mesenchymal transition. *Nat. Rev. Mol. Cell Biol.* **15**, 178–196.

Li, N.S., Zou, J.R., Lin, H., Ke, R., He, X.L., Xiao, L., Huang, D., Luo, L., Lv, N., and Luo, Z. (2016). LKB1/AMPK inhibits TGF β 1 production and the TGF β -signaling pathway in breast cancer cells. *Tumour Biol.* **37**, 8249–8258.

Luo, J., Hong, Y., Lu, Y., Qiu, S., Chaganty, B.K., Zhang, L., Wang, X., Li, Q., and Fan, Z. (2017). Acetyl-CoA carboxylase rewires cancer metabolism to allow cancer cells to survive inhibition of the Warburg effect by cetuximab. *Cancer Lett.* **384**, 39–49.

Malik, S.A., Mariño, G., BenYounès, A., Shen, S., Harper, F., Maiuri, M.C., and Kroemer, G. (2011). Neuroendocrine regulation of autophagy by leptin. *Cell Cycle* **10**, 2917–2923.

Mihaylova, M.M., and Shaw, R.J. (2011). The AMPK signalling pathway coordinates cell growth, autophagy and metabolism. *Nat. Cell Biol.* **13**, 1016–1023.

Minokoshi, Y., Kim, Y.B., Peroni, O.D., Fryer, L.G., Müller, C., Carling, D., and Kahn, B.B. (2002). Leptin stimulates fatty-acid oxidation by activating AMP-activated protein kinase. *Nature* **415**, 339–343.

- Protani, M., Coory, M., and Martin, J.H. (2010). Effect of obesity on survival of women with breast cancer: systematic review and meta-analysis. *Breast Cancer Res. Treat.* *123*, 627–635.
- Rajala, M.W., and Scherer, P.E. (2003). Minireview: the adipocyte—at the crossroads of energy homeostasis, inflammation, and atherosclerosis. *Endocrinology* *144*, 3765–3773.
- Rios, M., Foretz, M., Viollet, B., Prieto, A., Fraga, M., Costoya, J.A., and Señaris, R. (2013). AMPK activation by oncogenesis is required to maintain cancer cell proliferation in astrocytic tumors. *Cancer Res.* *73*, 2628–2638.
- Röhrig, F., and Schulze, A. (2016). The multifaceted roles of fatty acid synthesis in cancer. *Nat. Rev. Cancer* *16*, 732–749.
- Rompani, S.B., and Cepko, C.L. (2008). Retinal progenitor cells can produce restricted subsets of horizontal cells. *Proc. Natl. Acad. Sci. USA* *105*, 192–197.
- Santos, C.R., and Schulze, A. (2012). Lipid metabolism in cancer. *FEBS J.* *279*, 2610–2623.
- Simonsson, M., Kanduri, M., Grönroos, E., Heldin, C.H., and Ericsson, J. (2006). The DNA binding activities of Smad2 and Smad3 are regulated by co-activator-mediated acetylation. *J. Biol. Chem.* *281*, 39870–39880.
- Svensson, R.U., Parker, S.J., Eichner, L.J., Kolar, M.J., Wallace, M., Brun, S.N., Lombardo, P.S., Van Nostrand, J.L., Hutchins, A., Vera, L., et al. (2016). Inhibition of acetyl-CoA carboxylase suppresses fatty acid synthesis and tumor growth of non-small-cell lung cancer in preclinical models. *Nat. Med.* *22*, 1108–1119.
- Tevaarwerk, A.J., Gray, R.J., Schneider, B.P., Smith, M.L., Wagner, L.I., Fetting, J.H., Davidson, N., Goldstein, L.J., Miller, K.D., and Sparano, J.A. (2013). Survival in patients with metastatic recurrent breast cancer after adjuvant chemotherapy: little evidence of improvement over the past 30 years. *Cancer* *119*, 1140–1148.
- Toyama, E.Q., Herzig, S., Courchet, J., Lewis, T.L., Jr., Losón, O.C., Hellberg, K., Young, N.P., Chen, H., Polleux, F., Chan, D.C., and Shaw, R.J. (2016). Metabolism. AMP-activated protein kinase mediates mitochondrial fission in response to energy stress. *Science* *351*, 275–281.
- Tu, A.W., and Luo, K. (2007). Acetylation of Smad2 by the co-activator p300 regulates activin and transforming growth factor beta response. *J. Biol. Chem.* *282*, 21187–21196.
- Vander Heiden, M.G., Cantley, L.C., and Thompson, C.B. (2009). Understanding the Warburg effect: the metabolic requirements of cell proliferation. *Science* *324*, 1029–1033.
- Wang, C.C., Bajikar, S.S., Jamal, L., Atkins, K.A., and Janes, K.A. (2014). A time- and matrix-dependent TGFBR3-JUND-KRT5 regulatory circuit in single breast epithelial cells and basal-like premalignancies. *Nat. Cell Biol.* *16*, 345–356.
- Wang, M.D., Wu, H., Fu, G.B., Zhang, H.L., Zhou, X., Tang, L., Dong, L.W., Qin, C.J., Huang, S., Zhao, L.H., et al. (2016). Acetyl-coenzyme A carboxylase alpha promotion of glucose-mediated fatty acid synthesis enhances survival of hepatocellular carcinoma in mice and patients. *Hepatology* *63*, 1272–1286.
- Weigelt, B., Peterse, J.L., and van 't Veer, L.J. (2005). Breast cancer metastasis: markers and models. *Nat. Rev. Cancer* *5*, 591–602.
- Wu, M.H., Chou, Y.C., Chou, W.Y., Hsu, G.C., Chu, C.H., Yu, C.P., Yu, J.C., and Sun, C.A. (2009). Circulating levels of leptin, adiposity and breast cancer risk. *Br. J. Cancer* *100*, 578–582.
- Wu, C.L., Qiang, L., Han, W., Ming, M., Viollet, B., and He, Y.Y. (2013). Role of AMPK in UVB-induced DNA damage repair and growth control. *Oncogene* *32*, 2682–2689.
- Yung, R.L., and Ligibel, J.A. (2016). Obesity and breast cancer: risk, outcomes, and future considerations. *Clin. Adv. Hematol. Oncol.* *14*, 790–797.
- Zaidi, N., Swinnen, J.V., and Smans, K. (2012). ATP-citrate lyase: a key player in cancer metabolism. *Cancer Res.* *72*, 3709–3714.

STAR★METHODS

KEY RESOURCES TABLE

REAGENT or RESOURCE	SOURCE	IDENTIFIER
Antibodies		
Rabbit monoclonal anti-ACC1	Cell Signaling Technology	Cat#3662; RRID: AB_2219400
Rabbit monoclonal anti-pACC1	Cell Signaling Technology	Cat#3661; RRID: AB_330337
Rabbit monoclonal anti-ACLY	Cell Signaling Technology	Cat#13390
Rabbit monoclonal anti-AMPK	Cell Signaling Technology	Cat#5831; RRID: AB_10622186
Rabbit monoclonal anti-pAMPK	Cell Signaling Technology	Cat#2531; RRID: AB_330330
Rabbit monoclonal anti-pERK1/2	Cell Signaling Technology	Cat#9101; RRID: AB_331646
Rabbit monoclonal anti-pAKT	Cell Signaling Technology	Cat#9271; RRID: AB_329825
Rabbit monoclonal anti-pp38	Cell Signaling Technology	Cat#9211; RRID: AB_331641
Mouse monoclonal anti-pStat3	Cell Signaling Technology	Cat#9138; RRID: AB_331262
Rabbit monoclonal anti-Snail	Cell Signaling Technology	Cat#3879; RRID: AB_2255011
Rabbit monoclonal anti-Slug	Cell Signaling Technology	Cat#9585; RRID: AB_2239535
Rabbit monoclonal anti-Vimentin	Cell Signaling Technology	Cat#5741; RRID: AB_10695459
Rabbit monoclonal anti-N-Cadherin	Cell Signaling Technology	Cat#4061; RRID: AB_2077426
Rabbit monoclonal anti-E-Cadherin	Cell Signaling Technology	Cat#3195; RRID: AB_2291471
Rabbit monoclonal anti-Smad2/3	Cell Signaling Technology	Cat#8685; RRID: AB_10889933
Rabbit monoclonal anti-pSmad2	Cell Signaling Technology	Cat#3108; RRID: AB_490941
Rabbit monoclonal anti-TAK1	Cell Signaling Technology	Cat#5206; RRID: AB_10694079
Rabbit polyclonal anti-Histone H3	Cell Signaling Technology	Cat#2650; RRID: AB_2115124
Rabbit monoclonal anti-Tubulin	Cell Signaling Technology	Cat#5346; RRID: AB_1950376
Rabbit monoclonal anti-Actin	Cell Signaling Technology	Cat#12620
Rabbit monoclonal anti-GAPDH	Cell Signaling Technology	Cat#8884; RRID: AB_11129865
Rabbit polyclonal anti-Flag M2	Cell Signaling Technology	Cat#2368; RRID: AB_2217020
Mouse monoclonal anti-Acetyl-Lys	Cell Signaling Technology	Cat#9681; RRID: AB_331799
Rabbit monoclonal anti-Acetyl-Lys	Cell Signaling Technology	Cat#9441; RRID: AB_331805
Rabbit monoclonal anti-LKB1	Cell Signaling Technology	Cat#3050; RRID: AB_823559
Mouse monoclonal anti-VCP	Abcam	ab11433; RRID: AB_298039
Rabbit monoclonal anti-Leptin receptor	Abcam	ab5593; RRID: AB_304969
Rabbit polyclonal anti-Acetyl Histone H3	Millipore	06-599; RRID: AB_2115283
Mouse monoclonal anti-N-Cadherin	SantaCruz biotech	sc-271386; RRID: AB_10610922
Mouse monoclonal anti-Vimentin	SantaCruz Biotech	sc-32322; RRID: AB_628436
Rabbit polyclonal anti-CAMKK2	Atlas antibodies	HPA017389; RRID: AB_1845956
donkey anti-Rabbit IgG F(ab') ₂ fragment DyLight 405	Jackson ImmunoResearch	711-476-152; RRID: AB_2632566
donkey anti-mouse IgG F(ab') ₂ fragment Alexa Fluor 488	Jackson ImmunoResearch	715-545-150; RRID: AB_2340846
Normal rabbit IgG	Cell Signaling Technology	Cat#2729; RRID: AB_2617119
Biological Samples		
Human breast carcinoma metastatic tissue microarray, containing 48 cases of breast cancer, with 36 matched metastatic breast cancer and 12 normal tissue	US Biomax	BRM961
Human lung adenocarcinoma tissue array, with 30 matched tumor, normal adjacent tissue and positive lymph nodes	US Biomax	HLug-Ade090Lym-01
Chemicals, Peptides, and Recombinant Proteins		
Lipofectamine RNAiMax	Thermo Fisher Scientific	13778150
Lipofectamine 2000	Thermo Fisher Scientific	11668027
IP lyses buffer	Pierce	87787
Sodium butyrate	Sigma	B5887

(Continued on next page)

Continued

REAGENT or RESOURCE	SOURCE	IDENTIFIER
Protease inhibitor	Roche	11697498001
Phosphatase inhibitor	Roche	04906837001
BCA protein assay	Pierce	23225
ECL prime	Amersham	RPN2236
Protein G agarose beads	Cell Signaling Technology	Cat#9007
EnVission antibody Diluent	Dako	K8006
EnVission Dual link System-HRP	Dako	K4065
Tissue-Tek O.C.T	VWR	25608-930
To-Pro 3	Life technologies	T3605
Aqueous mounting medium	Dako	S3025
Anti-Flag M2 affinity gel	Sigma	A2220
3x Flag peptide	Sigma	F4799
G418	Sigma	G418-RO
Human Leptin	Peprotech	300-27
Murine leptin	Peprotech	450-31
Human TGF- β	Peprotech	100-21
Tofa	Sigma	T6575
C646 p300 inhibitor	Millipore	382113
(5Z)-7-Oxozeaenol TAK1 inhibitor	Sigma	O9890
PF-04691502 PI3K inhibitor	Sigma	PZ0235
PD-0325901 MEK1/2 inhibitor	Sigma	PZ0162
BMS 303141 ACLY inhibitor	Sigma	SML0784
Critical Commercial Assays		
Invasion assay inserts	Corning	3458
Migration assay inserts	Corning	3422
Acetyl-CoA assay kit	Sigma	MAK039
Experimental Models: Cell Lines		
Murine: e0771	ATCC	CR-2755
Murine: 4T1	ATCC	CRL-2539
Human: MDA-MB-231	ATCC	HTB-26
Human: MCF-7	ATCC	HTB-22
Human: T47D	ATCC	HTB-133
Human: HEK293T	ATCC	CRL-3216
Human: U2OS WT	Gift of Dr. Reuben Shaw	N/A
Human: U2OS AMPK DKO	Gift of Dr. Reuben Shaw	N/A
Experimental Models: Organisms/Strains		
Mouse: C57BL/6JRj	Janvier	N/A
Mouse: BALB/cJRj	Janvier	N/A
Mouse: BALB/cAnN-Foxn1 ^{nu/nu} /Rj	Janvier	N/A
Oligonucleotides		
esiEGFP	Sigma	EHUEGFP
esiMAP3K7	Sigma	EHU081791
esiSTK11	Sigma	EHU019041
esiCAMKK2	Sigma	EHU083851
esiPRKAA1	Sigma	EHU074041
esiPRKAA2	Sigma	EHU042081
esiACLY	Sigma	EHU081921

(Continued on next page)

Continued

REAGENT or RESOURCE	SOURCE	IDENTIFIER
Recombinant DNA		
pBabe RFP1-Smad2	Wang et al., 2014	Addgene Plasmid #58491
pBabe RFP-Smad2K3R	This paper	N/A
FUtdTW	Rompani and Cepko, 2008	Addgene Plasmid #22478
pWZL-Neo-Myr-Flag-MAP3K7 TAK1	Boehm et al., 2007	Addgene Plasmid #20520
pLKO shScrambled	Sigma	SHC002
pLKO shACC	Sigma	TRCN0000004766
pLKO shLeptin receptor	Sigma	TRCN0000453202
pBase	VectorBuilder	N/A
piggybac-Flag-ACC tdT neo	VectorBuilder	N/A
piggybac-Flag-ACC ^{S79A} tdT neo	VectorBuilder	N/A
piggybac-Flag-ACC ^{S79E} tdT neo	VectorBuilder	N/A
psPAX2	VectorBuilder	N/A
pMD2.G	VectorBuilder	N/A

CONTACT FOR REAGENT AND RESOURCE SHARING

Further information and requests for resources and reagents should be directed to and will be fulfilled by the Lead Contact, Stephan Herzig (stephan.herzig@helmholtz-muenchen.de).

EXPERIMENTAL MODEL AND SUBJECT DETAILS

Animal Studies

In each animal experiment, mice were randomly assigned to each group. Animal handling and experimentation was performed in accordance with the European Union directives and the German animal welfare act and approved by the Regierungspräsidium Karlsruhe, Germany.

All experiments were performed in 8 weeks old female mice (BALB/cJRj, C57Bl6/JRj and BALB/cAnN-*Foxn1*^{nu/nu}/Rj) obtained from Janvier labs and maintained on a 12h light dark cycle at 22°C.

Cell Culture

MCF-7 (human breast cancer cell line), e0771 and 4T1 (murine breast cancer cell lines) were maintained in RPMI no Phenol Red (GIBCO) supplemented with 10% fetal bovine serum (Millipore). MDA-MB-231, T47D (human breast cancer cell lines), HEK293T (human embryonic kidney cell line) and U2OS (human Osteosarcoma cell line) were maintained in Dulbecco's modified Eagle's medium (GIBCO) supplemented with 10% fetal bovine serum (Millipore). All cell lines were cultured at 37°C in 10% CO₂ incubator, and have been derived from murine or human female donors.

TMA

The human TMA paraffin sections of human breast carcinoma metastatic tissue microarray, containing 48 cases of breast cancer, with 36 matched metastatic breast cancer and 12 normal tissue (TMA BRM961), and human lung adenocarcinoma tissue array, with 30 matched tumor, normal adjacent tissue and positive lymph nodes (HLug-Ade090Lym-01) were obtained from US Biomax. All the information relative to the age/developmental stage, sex, and gender identity can be obtained at US Biomax webpage.

METHOD DETAILS

Cell Treatments

For ACC1 inhibition, cells were treated with 5 μM of Tofa during 24-48h. TGFβ 4ng/ml (Peprotech 100-21) treatment for 24h was used to stimulate EMT in breast cancer cell lines. Leptin treatment was performed using 100ng/ml of human leptin (Peprotech 300-27) or mouse leptin (Peprotech 450-31) during 3-5 days. Intracellular signaling pathways were inhibited by using (5Z)-7-Oxozeaenol TAK1 inhibitor (50nM) (Sigma O9890), PF-04691502 PI3K inhibitor (30nM) (Sigma PZ0235), PD-0325901 MEK1/2 inhibitor (20nM) (Sigma PZ0162), or BMS 303141 ACLY inhibitor (5μM) (Sigma SML0784). All these treatments were performed during 24h alone or in combination with Tofa, leptin or TGFβ at the concentrations mentioned above.

Animal Studies

For lung colonization experiments, 1×10^5 e0771 or MCF-7 cells were resuspended in 100 μ L of PBS and injected in the lateral tail vein of C57Bl6/JRj or BALB/cAnN-*Foxn1*^{nu/nu}/Rj female mice respectively. Three weeks after injection, the animals were sacrificed by cervical dislocation and lungs harvested and examined for lung macrometastases before paraffin embedding. For micrometastasis quantification, embedded lungs were sectioned (7 μ m) and stained with H&E, and six non-consecutive sections per sample were analyzed.

For the orthotopic breast cancer model, 4T1 cells (1×10^5) resuspended in 30 μ L were implanted in the third right mammary fat pad of BalB/cJRj female mice. Mastectomy was performed when the tumors reached 5mm in diameter, and three weeks after resection animals were sacrificed and lungs were collected for macro and micrometastasis quantification as described above.

Transfection and Infection

For the generation of stable breast cancer cell lines expressing Flag-ACC1, Flag-ACC1S79A or Flag-ACC1S79E we used the piggybac system. Cells were cotransfected in 6-well plates with 10 μ L of Lipofectamine 2000 combined with 100ng of pBase and 1 μ g of piggybac-Flag-ACC1 tdT neo, 1 μ g of piggybac-Flag-ACC^{S79A} tdT neo or 1 μ g of piggybac-Flag-ACC^{S79E} tdT neo. After transfection cells were selected with G418 (Sigma G418-RO) for 5 days.

For knockdown experiments, the different cell lines were transfected in 12-well plates with Lipofectamine RNAiMax combined with 10nM of the different esiRNA: esiEGFP (Sigma EHUEGFP), esiACLY (Sigma EHU081921), esiSTK11 (Sigma EHU019041), esiMAP3K7 (Sigma EHU081791), esiPRKAA1 (Sigma EHU074041), esiPRKAA2 (Sigma EHU042081) or siCAMKK2 (Sigma EHU083851). Forty-eight hours after transfection cells were treated as mentioned and after 24h cells were used for the corresponding assays.

For lentivirus generation, 1×10^6 HEK293T cells were seeded in 6-well plates in DEMEM 10% FBS the day before transfection. Cells were transfected by adding 200 μ L of Opti-MEM (GIBCO 31985062) containing 5 μ L of Lipofectamine 2000 (Invitrogen 11668027), 1 μ g of pLKO shscrambled, shLeptin receptor, shACC1, or FUtdTW combined with 1 μ g psPAX2 and 100ng pMD2.G. Twenty-four hours later, media was changed by DMEM 10% FBS containing 1.1% BSA. After 24h the supernatant was recovered, filtered with 0,45 μ m filters and used to infect breast cancer cell lines.

Migration/Invasion Assays

Transwell migration/invasion assays were performed in 6.5mm polycarbonate 8 μ m pore size membrane inserts uncoated (Corning 3422) or coated (Corning 3458). E0771 and 4T1 were treated with leptin for 3 days, and MCF-7, U2OS were treated with leptin or TGF β for 24h detached from the plates and 5×10^4 cells were resuspended in 0,5ml of serum free medium and plated in the upper chamber. The lower chamber was filled with 10% FBS medium and after 12h for 4T1 and 20h for e0771, MCF-7 and U2OS, cells were fixed in methanol, stained with crystal violet and migrating/invading cells were counted.

For invasion in 3D cultures, e0771, 4T1, T47D, MCF-7 and MDA-MB-231 were infected with lentivirus in order to express tdTomato (Adgene 22478). After selection, cells were grown in spheroids by the hanging drop protocol previously described (Foty, 2011). Three hundred cells of each line were seeded per drop and cells were maintain undisturbed for 3 days. Leptin 100ng/ml final concentration, Tofa, or siACC1 transfection media was added to the cells at day 3 and the cells were further grown for 48h. After the treatment, spheroids were recovered and seeded in a 2,2mg/ml collagen matrix in complete media. In the case of leptin or Tofa stimulation, these compounds were added to the collagen at 100ng/ml or 5 μ M final concentration, respectively. Pictures of the spheroids were taken every 24h until the experiment was finished. Invading areas were measured by using imageJ software in at least 10 spheroids and relative invasion represented.

Soft Agar Assays

e0771, 4T1, T47D, MCF-7 and MDA-MB-231 cells were treated with or without 100ng/ml leptin during 3 days. 5×10^4 of each cell line and condition were seeded by triplicate in 35mm plates containing DMEM 2x/RPMI no phenol red 2x, 10%FBS with 1,8% agarose in the bottom layer, and 0,7% agarose in the top layer including leptin in the corresponding groups. Cells were grown during 10 days, stained with crystal violet and colonies grown beyond 50 μ m in diameter were counted as positive.

Western Blot and Immunoprecipitation

Cells grown in the different conditions were lysed at 4°C in 300 μ L of IP lyses buffer (Pierce 87787) containing 5mM sodium butyrate (Sigma), protease inhibitors (Roche 11697498001) and phosphatase inhibitor (Roche 04906837001). Cell lysates were sonicated and centrifuged 14000x RPM for 5min 4°C. The supernatant was collected and protein concentration determined by BCA protein assay (Pierce 23225). Twenty-five μ g of total protein were subjected to SDS-PAGE electrophoresis, and transferred to a nitrocellulose membrane. After blocking, membranes were incubated overnight at 4°C with primary antibodies and with the appropriate secondary antibody for 1h at room temperature. Signals were detected with ECL prime (Amersham RPN2236), and visualized by Chemidoc Image System (BioRad) using ImageLab software.

For immunoprecipitation experiments, 400 μ g protein lysate was incubated for 1h at 4°C in lysis buffer containing 1%BSA and 20 μ L of protein G agarose beads (Cell Signaling Technology 9007). After centrifugation (14000x RPM 4°C) supernatants were collected and incubated with 5 μ g of the Smad2/3 antibody (Cell Signaling Technology 8685) or normal rabbit IgG (Cell Signaling Technology 2729) overnight at 4°C under rotation. Next day, 20 μ L of protein G agarose beads was added to the samples and

incubated for 4h at 4°C under rotation. Beads were washed 5 times with lysis buffer and proteins were eluted in SDS sample buffer and run by Western Blot. Twenty-five µg of protein lysate was running in parallel by Western Blot to check EMT markers and histone H3 acetylation.

Immunohistochemistry and Immunofluorescence

For the IHC in breast TMA (US Biomax BRM961) or lung TMA (US Biomax HLungA090Ly02), the paraffin sections were rehydrated and antigen retrieval was done in boiled 10mM sodium citrate pH6. The IHC was performed by overnight incubation at 4°C, using pACC1, N-Cadherin, E-Cadherin or pp38 antibodies in EnVission antibody Diluent (Dako K8006). The DAB staining was performed with EnVission Dual link System-HRP (Dako K4065) and samples were counterstained with hematoxylin, dehydrated and permanently coverslipped. The location of immunoreactivity, percentage of reactive area and intensity were determined and scored. To evaluate immunostaining intensity we used a numeric score ranging from 0 to 6.

Immunofluorescence was performed in spheroids grown in collagen 3D cultures as above. Collagen matrix containing the spheroids was fixed directly in the 96 well plates with 4% paraformaldehyde. The 3D cultures were cryoprotected by sequential incubation of 15% and 30% sucrose in PBS for 2h at 4°C with rotation. After removal of sucrose solution, 3D cultures were embedded in Tissue-Tek O.C.T (VWR 25608-930), frozen on dry ice for 30min and stored at –80°C until use. Sections of 8 µm were permeabilized by incubation with 0.5% Triton X-100 in PBS for 10min. After blocking, the slides were incubated with primary antibodies (Vimentin, N-Cadherin and pACC1) at 4°C overnight. Secondary antibodies, donkey anti-mouse IgG F(ab')₂ fragment Alexa Fluor 488 (Jackson ImmunoResearch 715-545-150) and donkey anti-Rabbit IgG F(ab')₂ fragment DyLight 405 (Jackson ImmunoResearch 711-476-152) were applied together with nuclear counterstaining To-Pro 3 (Life technologies T3605) and incubated for 1h at room temperature. All the washing steps were performed at room temperature for 10min in PBST. The slides were mounted with an aqueous mounting medium (Dako S3025) and pictures were taken under a fluorescence microscope.

CPT-1 and ACC1 activity

The CPT-1 activity assay was performed as previously described with minor modifications (Kaczor et al., 2005). Cells treated with or without leptin (100ug/ml) were lysed at 4°C in 300 µL of IP lyses buffer (Pierce 87787), and 300 µg of protein was added to a 96 well plate in triplicate and the same volume of 60mM tris HCL pH8, 1,5mM EDTA, 1,2mM L(-)carnitine, 0,25mM 5,5'-Ditiobis(2-nitrobenzoic acid) in a final volume of 250 µl. The reaction was initiated by adding 10 µL of 20 µM of palmitoyl-CoA (final concentration) and the absorbance at 412nm was followed for 10min at 30°C. The increase in absorbance was normalized by the negative control and represented as percentage of control.

4T1 cells overexpressing Flag-ACC1, Flag-ACC1S79A or Flag-ACC1S79E were lysed in IP buffer. 1mg of protein was subjected to immunoprecipitation with Anti-Flag M2 affinity gel (Sigma A2220) and processed as mentioned above. Flag-ACC1 was eluted in TBS containing 3x Flag peptide (Sigma F4799). After confirmation of equal amounts of protein by BCA assay and ACC1 by Western Blot, the samples were assayed for ACC1 activity. For each sample, the assay was made in triplicate by adding 20 µL of Flag IP to 180 µL of 100mM Tris HCL pH7.4, 0.3mM acetyl-CoA, 4mM ATP, 2mM MgCl₂, 1% BSA and 20mM NaHCO₃ at 37°C. The reaction was stopped with perchloric acid at various time points. The reduction in acetyl-CoA in the sample was measured with acetyl-CoA assay kit (Sigma MAK039) according to the manufacturer's instructions. The reduction of acetyl-CoA levels was taken as an indirect measure of ACC1 activity and represented as pM of malonyl-CoA/min.

Seahorse Analyses

MDA-MB-231, MCF-7, 4T1 and e0771 cells were pre-treated with 100ng/ml of leptin for 72h, and 20000 MDA-MB-231 and MCF-7 cells or 15000 4T1 and e0771 cells were seeded on XF96 PS multi-well plates. After overnight incubation, the media was replaced with assay media 1h before the assay. A mitochondrial stress test was performed according to manufacturer's instructions (Seahorse Bioscience). To perform the assay, 1 µM oligomycin, 1.5 µM FCCP, 0.5 µM rotenone and 0.5 µM actinycin A was added to the cells. Oxygen consumption rate was normalized to cell density determined by sulforhodamine B staining.

Acetyl-CoA Measurements

Cells were seeded in triplicates in 15cm dishes at 80% of confluence and treated as mentioned above. After treatment, cells were washed with cold PBS, scraped, sonicated and cellular protein was precipitated with PCA. After centrifugation, supernatant was recovered and neutralized by the addition of potassium bicarbonate until the pH of the sample was in the range of 6-8 and precipitates were removed by centrifugation. The supernatant was used to determine acetyl-CoA concentration in duplicate by using an Acetyl-CoA assay kit (Sigma MAK039) according to manufacturer's instructions.

QUANTIFICATION AND STATISTICAL ANALYSIS

Statistical Analysis

All data are presented as mean ± SEM and n is indicated for each experiment. Datasets were testing for normal variance and accordingly analyzed with GraphPad Prism software. Depending on the data Student's t test, one- or two-way ANOVA, or Mann-Whitney test were used for comparisons and indicated in the legends of each panel. Differences were considered significant at $p < 0.05$ and indicated on the panels as (*) $p < 0,05$, (**) $p < 0,005$.

Cell Metabolism, Volume 26

Supplemental Information

Acetyl-CoA Carboxylase 1-Dependent

Protein Acetylation Controls Breast

Cancer Metastasis and Recurrence

Marcos Rios Garcia, Brigitte Steinbauer, Kshitij Srivastava, Mahak Singhal, Frits Mattijssen, Adriano Maida, Sven Christian, Holger Hess-Stumpp, Hellmut G. Augustin, Karin Müller-Decker, Peter P. Nawroth, Stephan Herzig, and Mauricio Berriel Diaz

SUPPLEMENTAL DATA

SUPPLEMENTAL FIGURE LEGENDS

Figure S1. Leptin induces EMT and metabolic changes. Related to Figure 1. (A) Levels of LepR and (B) leptin in human and murine breast cancer cell lines. (n=3-4). (C) Relative cell numbers representing proliferation of different breast cancer cell lines under leptin treatment. (n=3). (D) Western Blot showing levels of EMT markers in breast cancer cell lines treated with leptin 100ng/ml. (n=3). (E) Colony formation in soft agar of breast cancer cell lines treated with 100ng/ml of leptin, represented as percentage of the control. (n=3) (F) 3D collagen invasion assay in MDA-MB-231 and MCF-7 (G) cells treated with 100ng/ml of leptin. (n=3). (H) mRNA levels of LepR in e0771 and 4T1 cells transfected with scrambled or LepR siRNA. (n=2). (I) Quantification of the western blot shown in Fig 1G (4T1 cells). (J) Invasion of 4T1 and (K) e0771 cells in trans-well assays. (n=2). (L) 4T1 invasion in 3D collagen cultures in the presence or absence of leptin. (n=3) (M) e0771 invasion in 3D collagen cultures in the presence or absence of leptin and (N) representative pictures. (n=3). (O) EMT markers in spheroids of e0771 cells (n=2). (P) Quantification of the immunohistochemistry staining of primary tumors generated by orthotopical injection of e0771 in C57Bl6/J mice from Fig 1D. All data in the figure are shown as the mean \pm s.e.m. n numbers refer to biological replicates. (F, G, J, K, L) 1-way ANOVA with Tukey's Multiple Comparison Posttest. (C,E,H,P) Student's t-test. (L) 2-way ANOVA with Bonferroni's Multiple Comparison Posttest. *P < 0.05, **P < 0.01, ***P < 0.001.

Figure S2. ACC regulates EMT and protein acetylation. Related to Figure 2. (A) Levels of total protein acetylation in 4T1 (low exposition from Fig2A), MCF-7, MDA-MB-231 and T47D breast cancer cells in the presence or absence of 100ng/ml of leptin. (n=3) (B) Western Blot quantification of total protein acetylation in breast cancer cell lines treated with or without 100ng/ml of leptin. (C) Quantification of the western blot shown in Fig 2C. (D) 3D collagen invasion assay of 4T1 cells carrying control or LepR shRNA, transfected with control or ACC1 siRNA. (n=3). All data in the figure are shown as the mean \pm s.e.m. n numbers refer to biological replicates. (C) 1-way ANOVA with Tukey's Multiple Comparison Posttest. (B) Student's t-test. *P < 0.05, **P < 0.01, ***P < 0.001.

Figure S3. Smad2 acetylation is downstream of ACC phosphorylation during EMT induction. Related to Figure 3. (A) Quantification of the western blot shown in Fig 3E. (B) IP of 4T1 cells treated with Tofa and C646 showing levels of Smad2 acetylation (C) Histone H3 acetylation and EMT markers in HEK293T cells transfected with empty vector, RFP-Smad2 wild-type or RFP-Smad2K3R and treated with TGF β or Tofa (n=4). (D) Western Blot of pACC, Histone H3 acetylation and EMT markers in 4T1 cells transfected with empty vector, RFP-Smad2 wild-type or RFP-Smad2K3R and treated with Leptin (n=2). Representative images shown.

Figure S4. TAK1 is the mayor kinase involve in AMPK-ACC phosphorylation during EMT induction. Related to Figure 4. (A) Densitometric analysis of pACC1 Western blot in Figure 4B, left panel (n=3). (B) Western blot showing levels of pACC and Snail in HEK293T cells transfected with empty vector or CA TAK1 and treated with TGF β . (C) Western blot of MCF-7 cells KD for LKB1 or (D) CAMKK2B showing changes in pACC under leptin or TGF β treatment (n=3). (E) Western Blot of EMT markers in MCF-7 cells transfected with esiEGFP, esiAMPKa1, esiAMPKa2 or esiAMPKa1/a2 and treated with Leptin or TGF β . Representative images shown.

Figure S5. ACC regulates invasion in vitro and metastasis in vivo. Related to Figure 4.

(A) Levels of EMT markers in control or ACC1 shRNA-carrying e0771, 4T1, MDA-MB-231 and T47D cell lines. (n=3) (B) Number of lung micrometastases per animal or in total in animals injected with wild-type or ACC1 knockdown e0771 cells into the tail vein. (6 mice per group) (C) *In vitro* ACC1 activity assay of wild-type ACC1, ACC1^{S79A} and ACC1^{S79E} (n=2). (D) Growth curves of 4T1 cells expressing wild-type ACC1 or ACC1^{S79A} (n=2). (E) Representative microphotographs of 4T1 cells transfected with empty vector, ACC1 wild-type or ACC1^{S79A}, showing morphological changes after TGFβ treatment. (F) Transwell invasion assay of 4T1 cells expressing ACC1^{S79E} in the presence or absence of leptin and TGFβ (n=2). (G) Western blot of 4T1 cells transfected with empty vector or ACC1^{S79E} in the presence or absence of TGFβ showing levels of EMT markers (n=2). (H) Western blot of MDA-MB-231 cells transfected with empty vector, ACC1 wild-type or ACC1^{S79A} in the presence or absence of TGFβ showing levels of EMT markers. (n=3). (I) Western blot of MDA-MB-231 cells transfected with empty vector, or ACC1^{S79A} and incubated for 24h in normoxia or hypoxia, showing levels of EMT markers. (J) Correlation of tumor size and number of lung micrometastases triggered by wild-type ACC1 or ACC1^{S79A}-carrying 4T1 cells injected into the mammary fat pad of BalbC mice. Linear regression ACC1^{S79A} R²= 0,357, ACC1^{S79E} R²= 0.06743 (7 mice per group). All data in the figure are shown as the mean ± s.e.m. n numbers refer to biological replicates. (B,D,F) 1-way ANOVA with Tukey's Multiple Comparison Posttest. *P < 0.05, **P < 0.01, ***P < 0.001.

Figure S1

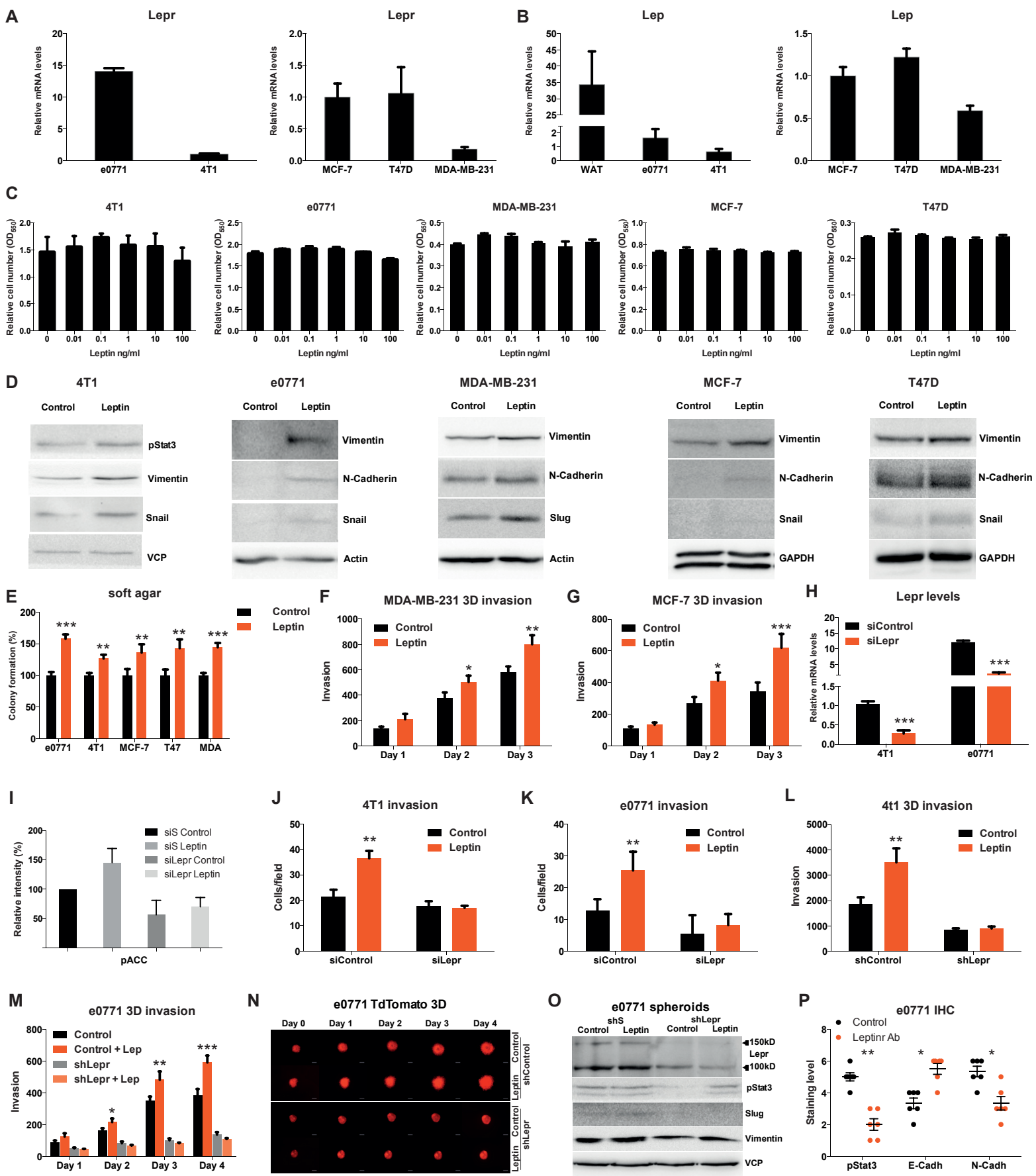
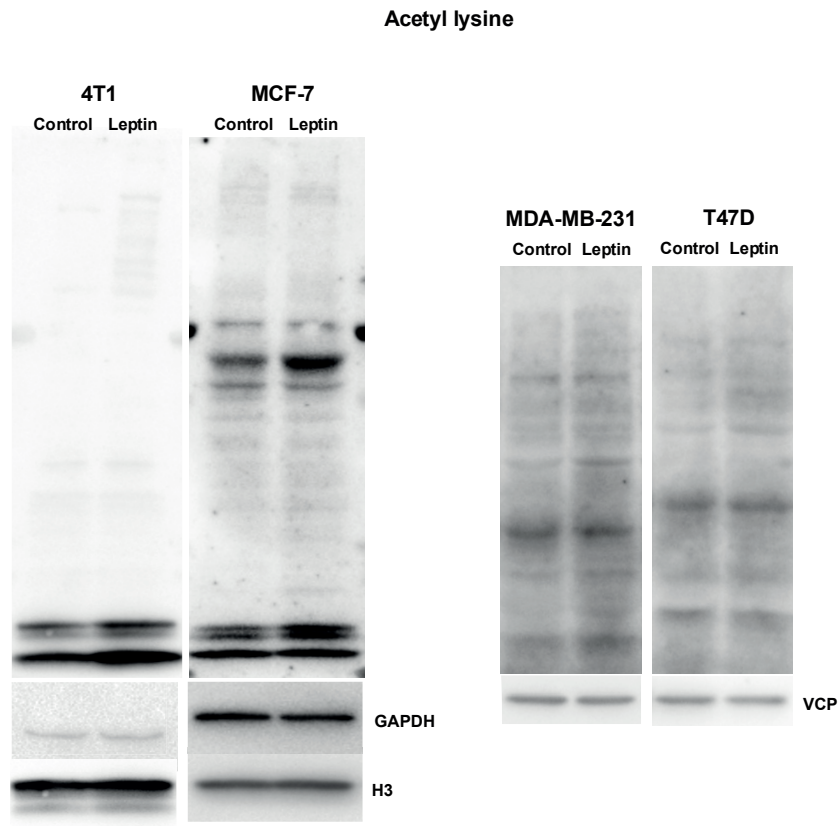
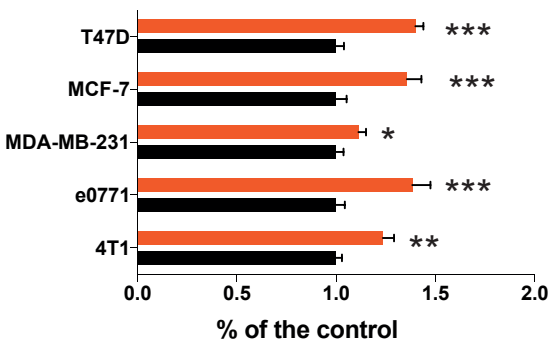


Figure S2

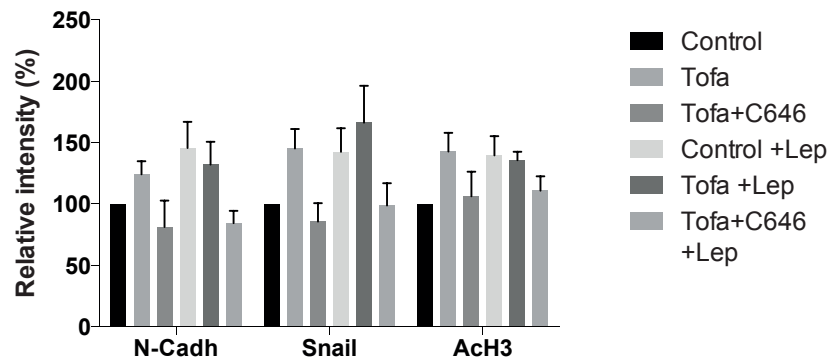
A



B



C



D

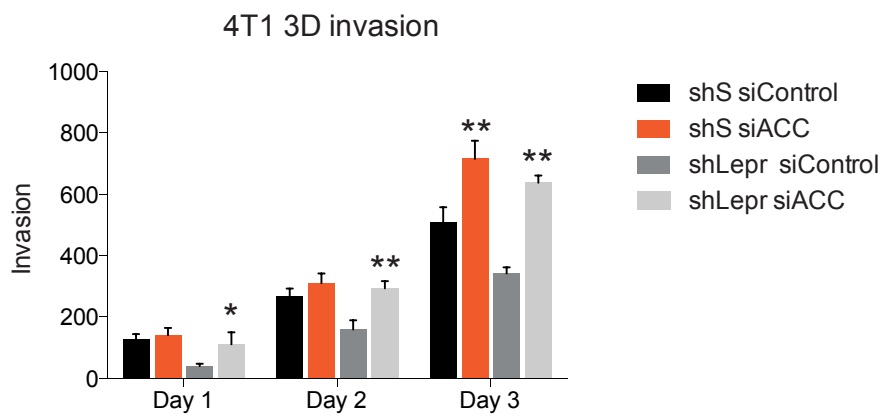
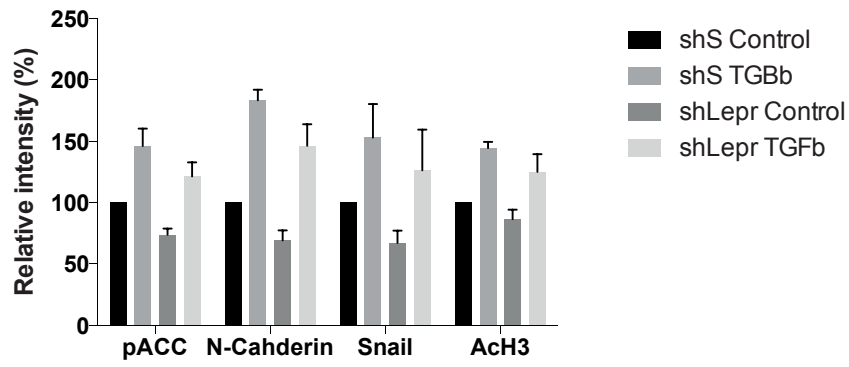
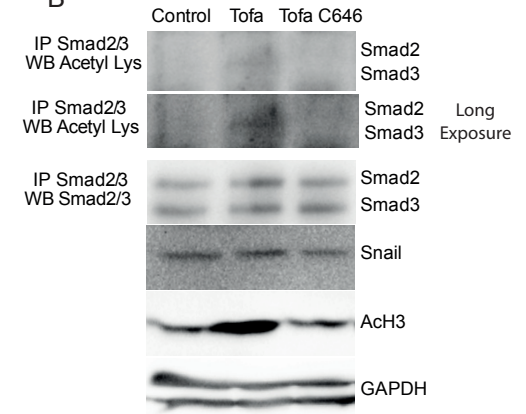


Figure S3

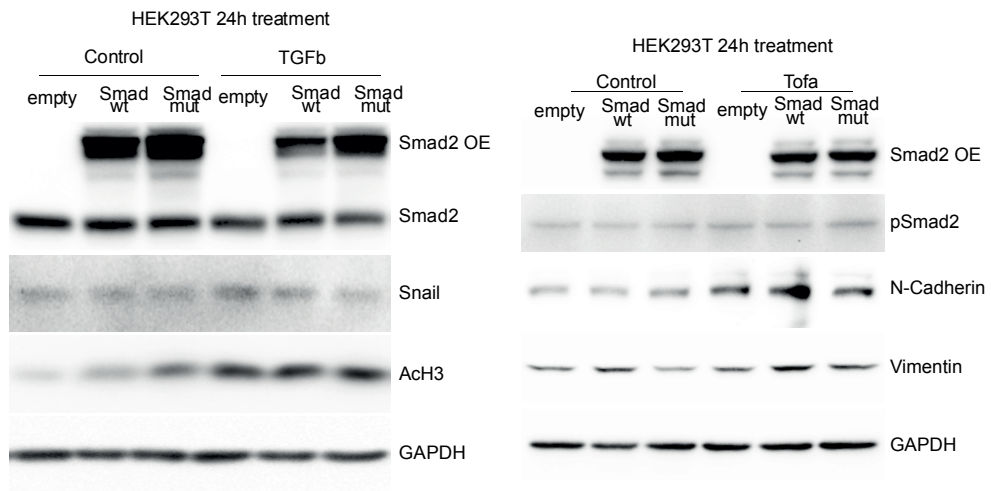
A



B



C



D

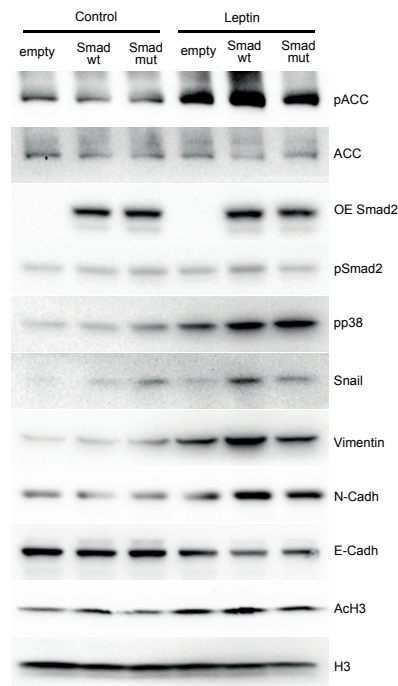


Figure S5

